

Neuron

A Designer AAV Variant Permits Efficient Retrograde Access to Projection Neurons

Highlights

- AAV can be endowed with robust retrograde functionality through directed evolution
- Up to two orders of magnitude increase in retrograde transport over existing variants
- Efficiency comparable to synthetic tracers
- Sufficient payload expression for circuit interrogation and gene manipulation

Authors

D. Gowanlock R. Tervo,
Bum-Yeol Hwang,
Sarada Viswanathan, ...,
Loren L. Looger, David V. Schaffer,
Alla Y. Karpova

Correspondence

schaffer@berkeley.edu (D.V.S.),
alla@janelia.hhmi.org (A.Y.K.)

In Brief

Projection neurons are a critical component of large-scale networks distributing the results of local circuit computations between distant brain regions, but their specific contribution is often hard to pinpoint because of the difficulty of gaining selective genetic access. Tervo et al. introduce a designer variant of adeno-associated virus, rAAV2-retro, that allows for efficient mapping, monitoring, and manipulation of projection neurons.

Accession Numbers

KX904530



A Designer AAV Variant Permits Efficient Retrograde Access to Projection Neurons

D. Gowanlock R. Tervo,¹ Bum-Yeol Hwang,^{2,6} Sarada Viswanathan,¹ Thomas Gaj,² Maria Lavzin,^{1,3} Kimberly D. Ritola,¹ Sarah Lindo,¹ Susan Michael,¹ Elena Kuleshova,^{1,5} David Ojala,² Cheng-Chiu Huang,^{1,7} Charles R. Gerfen,^{1,4} Jackie Schiller,^{1,3} Joshua T. Dudman,¹ Adam W. Hantman,¹ Loren L. Looger,¹ David V. Schaffer,^{2,*} and Alla Y. Karpova^{1,8,*}

¹Janelia Research Campus, Howard Hughes Medical Institute, Ashburn, VA 20147, USA

²Department of Chemical Engineering and Helen Wills Neuroscience Institute, University of California, Berkeley, Berkeley, CA 94720, USA

³Department of Physiology, Technion Medical School, Bat-Galim, Haifa 3525433, Israel

⁴Laboratory of Systems Neuroscience, National Institute of Mental Health, Bethesda, MD 20892, USA

⁵Institute of Higher Nervous Activity and Neurophysiology of the Russian Academy of Sciences, Moscow 117485, Russia

⁶Present address: 4D Molecular Therapeutics, Emeryville, CA 94608, USA

⁷Present address: TLC Biopharmaceuticals, Inc., South San Francisco, CA 94080, USA

⁸Lead Contact

*Correspondence: schaffer@berkeley.edu (D.V.S.), alla@janelia.hhmi.org (A.Y.K.)

<http://dx.doi.org/10.1016/j.neuron.2016.09.021>

SUMMARY

Efficient retrograde access to projection neurons for the delivery of sensors and effectors constitutes an important and enabling capability for neural circuit dissection. Such an approach would also be useful for gene therapy, including the treatment of neurodegenerative disorders characterized by pathological spread through functionally connected and highly distributed networks. Viral vectors, in particular, are powerful gene delivery vehicles for the nervous system, but all available tools suffer from inefficient retrograde transport or limited clinical potential. To address this need, we applied *in vivo* directed evolution to engineer potent retrograde functionality into the capsid of adeno-associated virus (AAV), a vector that has shown promise in neuroscience research and the clinic. A newly evolved variant, rAAV2-retro, permits robust retrograde access to projection neurons with efficiency comparable to classical synthetic retrograde tracers and enables sufficient sensor/effector expression for functional circuit interrogation and *in vivo* genome editing in targeted neuronal populations.

INTRODUCTION

Brain functions such as perception, cognition, and the control of movement depend on the coordinated action of large-scale neuronal networks, local circuit modules linked together by long-range connections (Miller and Vogt, 1984; Tomioka et al., 2005; Ramón y Cajal, 1911). Such long-range connections are formed by projection neurons that often comprise several intermingled classes, each projecting to a distinct constellation of downstream targets. Projection neurons have also been impli-

cated in the spread of several neurodegenerative diseases from spatially localized sites of onset (Guo and Lee, 2014; Seeley et al., 2009). Thus, the ability to selectively target specific classes of projection neurons for transgene delivery (e.g., for activity monitoring or manipulation, or genome editing for targeted gene knockouts or repair of pathological mutations) will be important both for gaining insights into how large-scale networks contribute to brain function and, in the long run, for therapeutic intervention in neurodegenerative diseases.

Viral vectors constitute an important class of tools for introducing transgenes into specific neuronal populations and are by far the best option for genetic access to target projection neurons through entry at axonal terminals and retrograde transport of their payload to the cell nuclei. A number of naturally evolved neurotropic viruses exhibit retrograde spread as part of their life cycle, including rabies (Baer et al., 1965; Callaway and Luo, 2015; Wickersham et al., 2007), poliovirus (Ohka et al., 1998), and herpes simplex virus (HSV) (Ugolini et al., 1987), among others. Of these, rabies virus is particularly neuro-invasive (Coulon et al., 1989) and quickly propagates through the nervous system through transcellular transfer (Kelly and Strick, 2000). However, its potential for both biological investigation and gene therapy is hampered by excessive virulence (Schnell et al., 2010), though progress is being made to reduce its toxicity (Reardon et al., 2016). In addition to naturally neurotropic strains, many other viruses can infect neurons when administered directly to the nervous system, with “pseudorabies” (SuHV1, actually a herpesvirus), adenoviruses, and lentiviruses used most commonly in animal research. Canine adenovirus-2 (CAV-2) displays the best infectivity and retrograde transport of this class of viruses (Soudais et al., 2001) and has increasingly become the reagent of choice for accessing projection neurons (Junyent and Kremer, 2015). However, CAV-2 permits only modest levels of transgene expression, displays some toxicity (Piersanti et al., 2013; Simão et al., 2016), and is currently not easily compatible with scalable, robust production for the generation of clinical-grade or even large animal studies (Kremer et al., 2000). Thus, the development of a non-toxic, readily

manufactured viral vector that affords flexible packaging of different transgenes, is robustly internalized and retrogradely transported by axons, and supports long-term, high-level payload expression remains a pressing need.

Recombinant adeno-associated viruses (rAAVs) have emerged as an effective platform for in vivo gene therapy, as they mediate high-level transgene expression, are non-toxic, and evoke minimal immune responses (Kaplitt et al., 2007). These properties were at the core of the decision to grant the first full regulatory approval of any gene therapy treatment to rAAV-mediated restoration of lipoprotein lipase deficiency (Gaudet et al., 2010). rAAVs hold great promise in clinical trials for a range of neurological disorders (Ojala et al., 2015), and they constitute some of the most widespread vectors in neuroscience research (Murlidharan et al., 2014). Since the original discovery that AAV can undergo retrograde transport (Kaspar et al., 2002), rAAVs have afforded some degree of retrograde access to projection neurons in select circuits (Castle et al., 2014; Hollis et al., 2008; Kaspar et al., 2002, 2003; Rothermel et al., 2013; Taymans et al., 2007; Towne et al., 2010), but their natural propensity for retrograde transport is low, hampering efforts to address the role of projection neurons in circuit computations or disease progression. Here we describe the in vivo directed evolution (Kotterman and Schaffer, 2014) of a new rAAV variant (rAAV2-retro) that, in addition to its regular ability to infect neuronal cell bodies at the site of exposure, is robustly internalized by axons and mediates retrograde access to projection neurons with efficiency comparable to classical retrograde labeling reagents such as synthetic dyes. The rAAV2-retro gene delivery system can be used on its own or in conjunction with Cre recombinase driver lines to achieve long-term, high-level transgene expression that is sufficient for effective functional interrogation of neural circuit function, as well as for genome editing in targeted neuronal populations.

RESULTS

Directed Evolution of rAAV2-retro

To engineer novel rAAVs with enhanced retrograde transport, we designed an in vivo directed-evolution approach to enrich for rAAV capsid variants that were efficiently transported to cell bodies of neurons sending long-range projections to the site of virus injection in the mouse brain (Figure 1A; Experimental Procedures). To maximize the likelihood of recovering a variant with the desired properties, we started with a diverse mixture of previously described libraries of rAAV *cap* variants (Koerber et al., 2006, 2008, 2009; Müller et al., 2003). Viral particles were packaged in a way that linked each capsid variant to the AAV genome containing the corresponding *cap* gene, and the final pool of capsid variants included point mutants, variants with a random 7-mer (plus three constant flanking residues) peptide insertion into the region AAV2 utilizes to bind its co-receptor heparin (Kern et al., 2003), and random chimeras of capsid gene sequences from seven parental serotypes (Figure 1A; Experimental Procedures). To identify variants with broad retrograde tropism, we targeted two independent populations of projection neurons: striatal GABAergic neurons projecting to substantia nigra pars reticulata (SNr) and glutamatergic hindbrain neurons

projecting to the cerebellar cortex. Three weeks following injection of the entire pool of rAAV variants into the SNr or cerebellum (one injection per animal), striatal or hindbrain tissue, respectively, was removed, the *cap* sequences were recovered by PCR, and virus was repackaged (Figure 1B). After two more selection steps, error-prone PCR was performed to further diversify the library, followed by two final in vivo selection steps.

We sequenced 30 *cap* variants after the fourth round of evolution, and the majority originated from the insertion library and contained exogenous 10-mer peptides between N587 and R588 of the wild-type AAV2 VP1 capsid gene (Müller et al., 2003) (see Experimental Procedures). Intriguingly, all of the recovered inserts were of the form LAxxDxTKxA or LAxDxTKxxA; mutations elsewhere in the sequence were also enriched (Table S1, available online). We sequenced a further 22 clones after the fifth round of evolution, and with this additional round of evolution, all sequences were AAV2 mutants with LAxxDxTKxA/LAxDxTKxxA insertions (Table S1), demonstrating a marked degree of further convergence. Such convergence suggested that specific peptide insertions into the heparin-binding loop were largely responsible for the retrograde functionality, with potential secondary contributions from the other sites (see Discussion).

We next focused a secondary screen (data not shown) on seventeen isolated variants possessing different combinations of peptide insertions and point mutations in the capsid sequence. To apply a high level of stringency, the chosen variants were packaged with an EGFP transgene driven by the CMV promoter, which is typically weak in neurons. For each capsid variant, we evaluated its ability to deliver sufficient payload to cell bodies in key afferent regions to permit the detection of non-antibody-amplified EGFP signal 3 weeks after injection. The clone (insert LADQDYTKTA + V708I + N382D) that displayed the strongest retrograde transport in two independent circuits in this secondary screen (cortex to globus pallidus and inferior olive/basal pontine nuclei [BPN] to cerebellum) was chosen for further analysis and named rAAV2-retro. When we assessed two additional promoters more commonly used in rodent in vivo studies (CAG; Figure 1B; or human *Synapsin-1*; data not shown), we observed remarkable retrograde labeling efficiency with this rAAV variant in a range of different circuits in mice and rats (Figures 1B and S1; Movie S1; see below). Swapping the 7-mer insertion to one of the other recovered sequences or adding additional point mutations identified in the screen did not lead to further increases in retrograde transport (data not shown).

Efficient Retrograde Access to Projection Neurons

The corticopontine tract is a remarkably convergent descending motor pathway, contributing more than 95% of the afferents to the BPN (Brodal and Bjaalie, 1992). This pathway is therefore particularly advantageous for quantifying the efficiency of viral uptake and retrograde transport by axonal terminals of projection neurons. Indeed, injection of rAAV2-retro into the BPN resulted in dense labeling of layer V neurons (Figure 2A), consistent with past tracing studies (Legg et al., 1989).

We therefore next compared the efficacy of retrograde transport in the corticopontine circuit for rAAV2-retro versus several

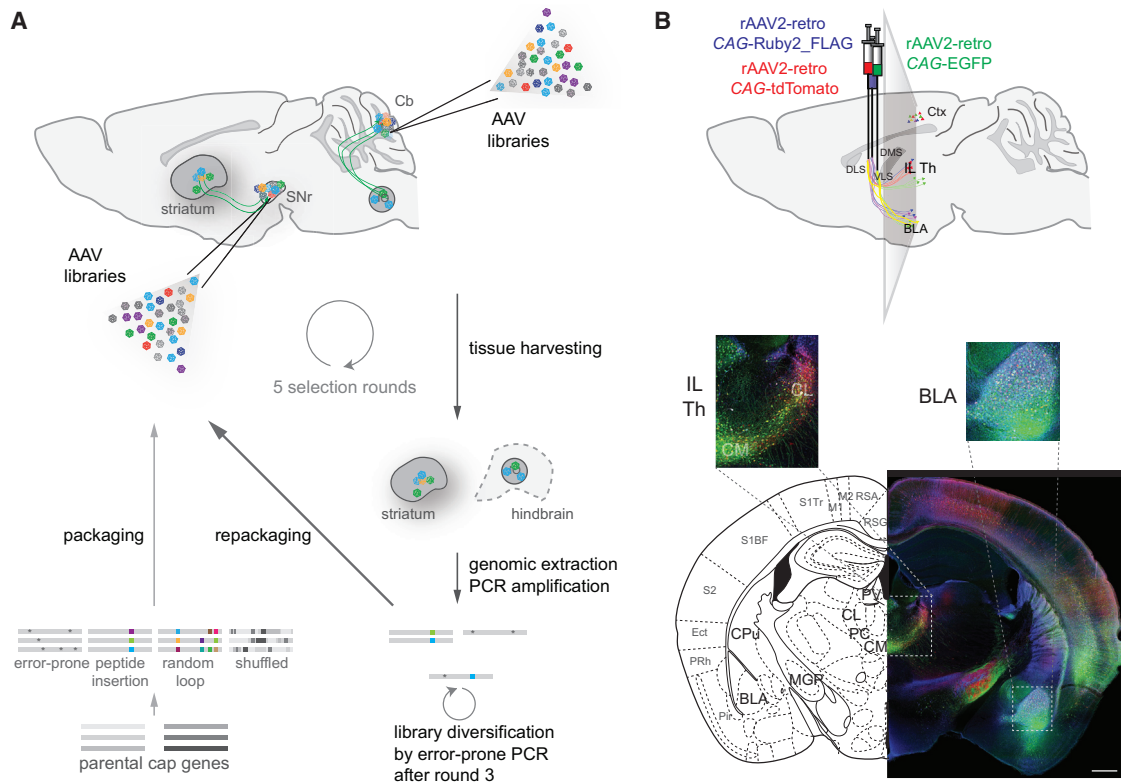


Figure 1. Directed Evolution of rAAV2-retro

(A) Schematic of the directed-evolution procedure. Plasmid libraries containing variant AAV *cap* genes previously generated by error-prone PCR, peptide insertion, randomization of loop regions, and DNA shuffling were packaged, and the resulting viral vector libraries were injected into substantia nigra or cerebellar cortex. Three weeks later, striatal or hindbrain, respectively, tissues were removed, viral genomes isolated, and selected *cap* genes amplified and packaged for the next round of selection. SNr, substantia nigra pars reticulata; IO, inferior olive; Cb, cerebellum.

(B) Example retrograde labeling of projection neurons with the final chosen variant, rAAV2-retro. Retrograde access to intermingled sub-populations of neurons in various brain regions projecting to three striatal compartments was assessed 2 weeks after delivery of rAAV2-retro carrying different fluorescent proteins into the corresponding axonal fields. rAAV2-retro tdTomato was injected into dorsolateral striatum (DLS), rAAV2-retro Ruby2_FLAG into dorsomedial striatum (DMS), and rAAV2-retro EGFP into ventrolateral striatum (VLS). Unlike in subsequent experiments (see Figures 2, 3, 4, 5, and 6), the three probes were visualized by immunohistochemistry to ensure robust detection of retrograde transport at this early time point. Ctx, cortex; BLA, basolateral amygdala; IL Th, intralaminar thalamic nuclei; CL, centrolateral thalamic nucleus; CM, centromedial thalamic nucleus. Scale bar, 1 mm. See also Figures S1 and S4 and Movie S1.

commonly used AAV serotypes, under identical infection and processing conditions (Figures 2B–2D; Experimental Procedures). To ensure quantification accuracy and to eliminate the possible confound of cell-to-cell variability in transgene expression level, we used the AAV to deliver Cre recombinase to *Rosa26-Lox-STOP-Lox-H2B-EGFP* (histone-fused EGFP) transgenic mice (He et al., 2012). Even a low concentration of the Cre enzyme is sufficient to turn on the expression of such a Cre-dependent cassette (Nagy, 2000), and the stringent nuclear localization of the histone-fused reporter affords unambiguous identification of infected cells, without confounding neuropil signal.

We used a semi-automated analysis procedure to calculate the linear density of infected cortical projection neurons in imaged sagittal sections from mouse brains harvested 3 weeks after local virus injection in the BPN (Figure 2C; Experimental Procedures). For animals infected with rAAV2, we observed minimal cortical GFP expression (linear density 0.98 ± 0.20

neurons/mm, mean \pm SEM, $n = 5$; Figure 2B, middle panel). In contrast, and in agreement with the earlier observation (Figure 2A), a dense layer of EGFP-positive layer V projection neurons could be observed throughout the rostro-caudal axis of the cortex in rAAV2-retro-injected animals (linear density, 130.11 ± 11.08 neurons/mm, $n = 4$; Figure 2B, lower panel). None of the other commonly used AAV serotypes, nor CAV-2, matched the retrograde efficiency of the engineered rAAV2-retro variant (linear densities, AAV1, 0.05 ± 0.04 ; AAV2, 0.98 ± 0.2 ; AAV5, 2.38 ± 1.24 ; AAV8, 1.43 ± 1.43 ; AAV9, 1.98 ± 0.86 ; DJ, 24.82 ± 14.32 ; CAV-2, 5.56 ± 4.13 ; $n = 3$ –5 each; Figures 2D and S2). The poor performance by the common AAV serotypes could not have arisen simply as a result of differences in infectivity since even the serotypes displaying similar labeling efficiency at the injection site to that of rAAV2-retro (rAAV2 and rAAV9) did not permit efficient retrograde access to corticopontine neurons (Figure S3). Strikingly, the density of cortical projection neurons labeled by rAAV2-retro was comparable to that

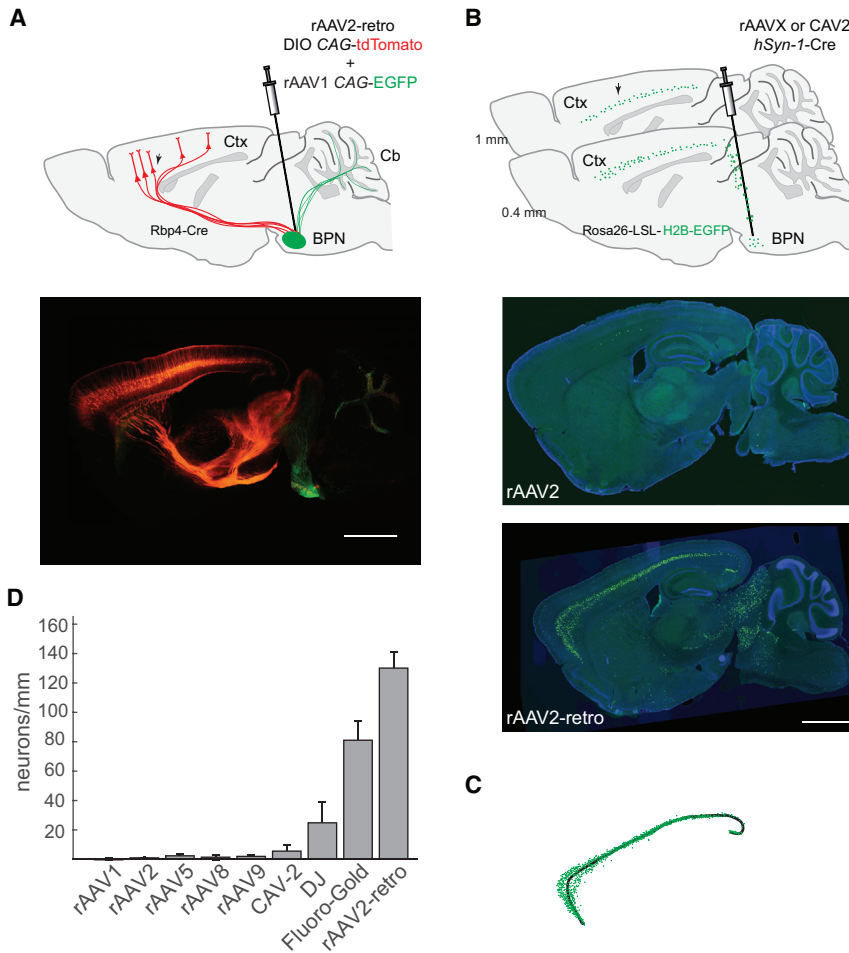


Figure 2. Quantification of Retrograde Transport Efficiency

(A) Efficient labeling of the corticopontine tract throughout the rostro-caudal axis via basal pontine injection of rAAV2-retro-DIO-CAG-tdTomato in a layer V-specific Cre mouse line (*Rbp4_KL100* Cre). Top panel: schematic of the experiment. Injection site was marked by co-injecting rAAV1-CAG-EGFP. BPN, basal pontine nuclei. Bottom panel: unamplified tdTomato and EGFP expression 3 weeks after injection. Scale bar, 1 mm. DIO, double-floxed inverted orientation.

(B) Quantification assay design. Top panel: schematic of the experiment. Corticopontine labeling was assessed in sagittal sections lateral to the injection tract (~1 mm lateral with respect to midline) taken from *Rosa26-Lox-STOP-Lox-H2B-EGFP* animals injected in the BPN with various AAV serotypes carrying Cre recombinase transgene. Arrow indicates expected nuclear GFP labeling in cortical neurons of the corticopontine tract. Middle panel: representative image of an rAAV2-injected brain. Bottom panel: representative image of rAAV2-retro-injected brain. Scale bar for both panels, 1 mm.

(C) Schematic of the semi-automated quantification procedure. Fluorescent nuclei (green) were automatically detected and counted along a manually drawn line that traced the length of cortical layer V (black).

(D) Retrograde transport efficiency for different AAV serotypes and for canine adenovirus type 2 (CAV-2) (see [Experimental Procedures](#)). Error bars represent the SEM. See also [Figures S2](#) and [S3](#).

achieved with Fluoro-Gold ([Schmued and Fallon, 1986](#)), a robust synthetic retrograde tracer (linear density, 81.03 ± 11.08 neurons/mm, $n = 3$). Thus, rAAV2-retro exhibits up to two orders of magnitude enhancement over existing serotypes in retrograde access to corticopontine projection neurons and rivals the efficacy of synthetic retrograde tracers.

Generality of Retrograde Functionality

We next examined whether the retrograde functionality of rAAV2-retro extended to other circuits, specifically by characterizing the extent to which it labeled various afferents to the dorsomedial striatum (DMS), a part of the basal ganglia that receives long-range inputs from a variety of cortical and subcortical areas ([Pan et al., 2010](#)). We found that the efficacy of rAAV2-retro-mediated retrograde access to the strongest afferent inputs into DMS—cortex, thalamus, and amygdala—was comparable to that of fluorescent beads classically used for retrograde tracing ([Figure 3A](#)). To provide an unbiased estimate for the number of retrogradely labeled neurons in all brain areas known to provide significant long-range input to the DMS, we next assigned any detected fluorescent label in an imaged section of the mouse brain to specific brain areas by aligning the section to the annotated Allen Brain Atlas ([Figures](#)

[3B](#) and [3C](#)). Quantitative analysis ([Figures 3B](#) and [3C](#)) revealed that strong retrograde labeling was found in the vast majority of regions that have been previously reported to send prominent projections to the striatum ([Pan et al., 2010](#)). In one noticeable exception, only modest labeling was observed in the substantia nigra pars compacta (SNc), despite it being the source of strong dopaminergic input to the DMS ([Figure 3C](#), arrow at cell count for SNc). A small subset of projection neuron classes was found to be similarly refractory to retrograde access by rAAV2-retro in some of the other circuits tested ([Table S2](#); note that all other AAV serotypes tested also failed to label these projections). Despite these exceptions, rAAV2-retro is broadly applicable for retrograde access to projection neurons within the CNS. We note that no rAAV2-retro-mediated labeling of unexpected pathways has been reported to date ([Table S2](#)); however, additional studies will be necessary to fully rule out its ability to infect axons of passage.

Retrograde Access to Genetically Defined Neuronal Populations

We also determined whether the retrograde functionality of rAAV2-retro could be combined with the specificity of Cre transgenic lines to enable the interrogation of specific classes of

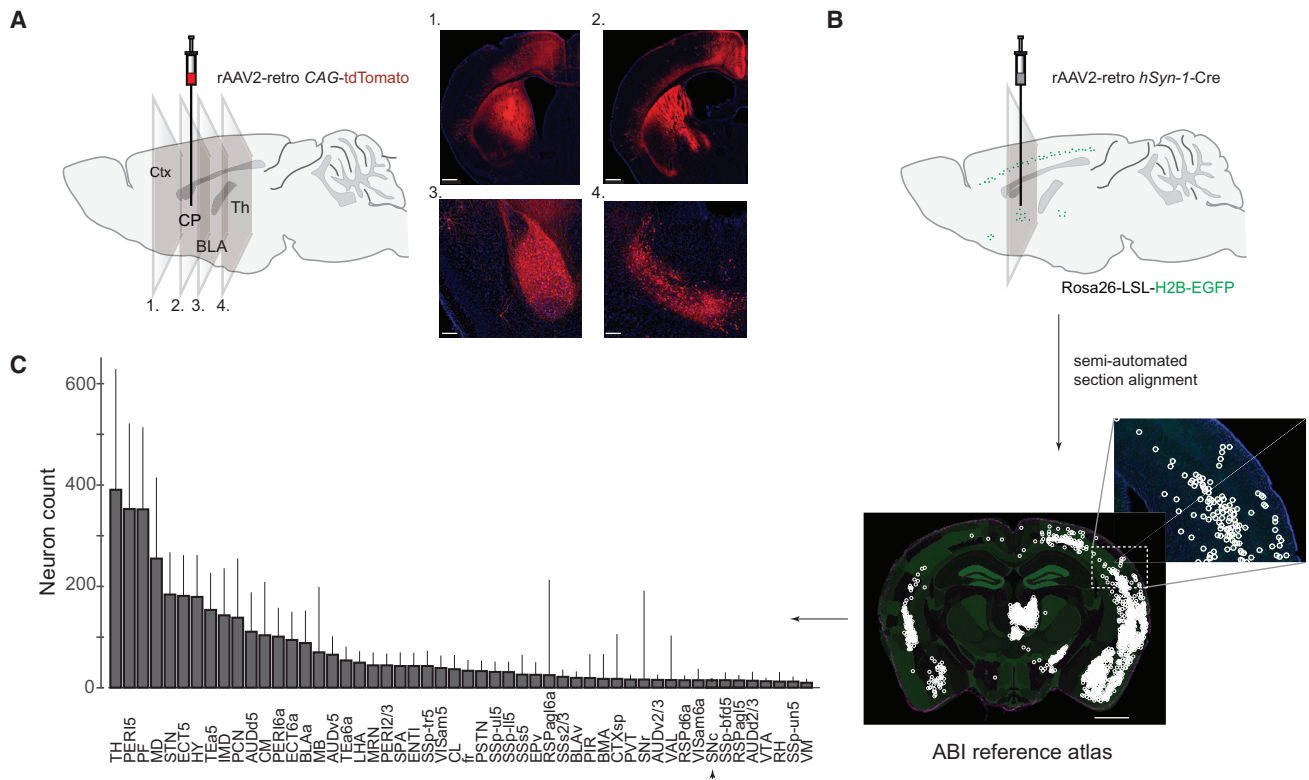


Figure 3. Generality of Retrograde Transport Afforded by rAAV2-retro

(A) Representative images showing extensive labeling in the main input structures to the dorsal striatum, including cortex (panel 1), amygdala (panel 3), and thalamus (panel 4). Scale bars, 800 (panels 1 and 2) and 2,200 μm (panels 3 and 4). Ctx, cortex; CP, caudate/putamen; BLA, basolateral amygdala; Th, thalamus.

(B) Schematic of automated whole-brain quantification of retrograde labeling. Brains of *Rosa26-LSL-H2B-EGFP* injected with rAAV2-retro-*hSyn1-Cre* were imaged to visualize DAPI-stained nuclei and green fluorescence from H2B-GFP-expressing nuclei. The green channel was used to detect labeled neurons; the blue channel was aligned to the Nissl images from the Allen Brain Institute's standard mouse brain (see [Experimental Procedures](#)). The alignment permitted detected neurons to be assigned to different regions using the annotation provided by the brain atlas. Scale bar, 1.25 mm.

(C) Whole-brain quantification of retrograde labeling out of a small region of the DMS. Abbreviations for the different brain areas are given according to the Allen Brain Atlas. Arrow highlights the SNc. Error bars represent the SEM.

projection neurons. Specifically, we asked whether we could combine rAAV2-retro and Cre transgenic lines to segregate two functionally distinct long-range connections that run in parallel between two brain areas. Projections from cerebral cortex to the striatum arise primarily from neurons in layer V, but some neurons in layers II and III also provide striatal inputs. It has been suggested that inputs to the striatum from different cortical layers constitute separate pathways, with neurons in layer V projecting to the patch compartment of the striatum and neurons in layers II and III to the matrix (Gerfen, 1989). The interdigitated nature of patch and matrix micro-compartments makes it difficult to selectively target these pathways for functional interrogation with the rAAV2-retro system alone. We therefore explored whether we could segregate the two inputs by combining rAAV2-retro with a transgenic line that expresses Cre recombinase in most layer V neurons (Gerfen et al., 2013), but not in neurons in layers II and III (Figure 4A).

To highlight both pathways in the same experiment, we chose a Cre-dependent color-flipping payload, which expresses tdTomato in the absence of Cre, but inverts to drive the expres-

sion of EGFP in Cre-positive cells (Saunders et al., 2012). When rAAV2-retro carrying this payload was injected into the DMS of a layer V-specific Cre driver line, *Rbp4_KL100 Cre* (Gerfen et al., 2013), layer V, but not layer II/III, neurons projecting to the striatum were robustly labeled with EGFP. Furthermore, the corticostriatal pathway originating in layer II/III was clearly distinguishable by the expression of tdTomato (Figure 4B). In accordance with the topographic nature of the corticostriatal projection, highly localized injections of the virus into the DMS led to labeling of correspondingly small sections of the cortex. Cortical regions with selective layer II/III labeling were not observed, however, suggesting that the two pathways from the same cortical area traverse through the neighboring matrix and patch micro-compartments within striatum.

While this experiment highlighted both pathways, choosing a “Cre-on” or a “Cre-off” payload will permit selective interrogation of one at the exclusion of the other. This example, therefore, highlights the added specificity of circuit interrogation that can be achieved by combining a highly efficient retrograde virus with available Cre (or Flp) driver lines.

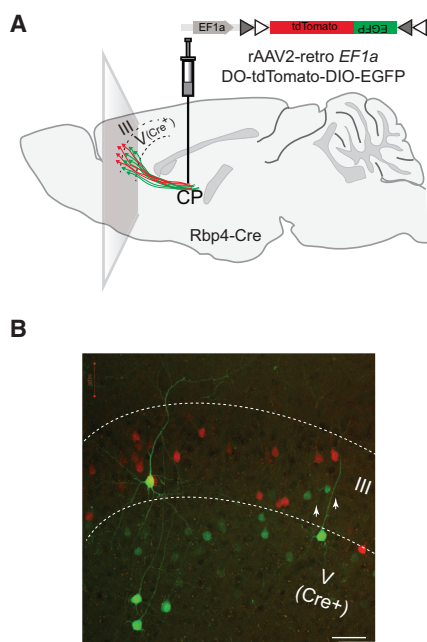


Figure 4. Combining rAAV2-retro System with Cre Driver Lines for Selective Access to Parallel Corticostriatal Pathways

(A) Schematic of the experiment. rAAV2-retro carrying a Cre-dependent color-flipping fluorescent reporter was injected into the striatum of a cortical layer V-specific Cre line. DO, double-floxed orientation; DIO, double-floxed inverted orientation.

(B) Two corticostriatal pathways differentially labeled through a Cre-dependent inversion of the reporter in one (layer V), but not the other (layer II/III), pathway. A presumed Cre-independent inversion—typical for all AAV vectors—was observed in a small fraction of corticostriatal neurons in layer II/III (white arrows). Scale bar, 50 μm .

Using rAAV2-retro for Circuit Interrogation and Gene Manipulation

The utility of rAAV2-retro for circuit interrogation will depend on its ability to mediate high levels of expression of genetically encoded indicators and effectors. We first assessed the ability to monitor neural activity in defined classes of projection neurons, through rAAV2-retro-mediated expression of GCaMP6f (Chen et al., 2013) (Figures 5A–5C). Using in vivo two-photon Ca^{2+} imaging, we detected dendritic and somatic Ca^{2+} transients in the primary motor cortex as early as 7 days after viral delivery to the BPN (Figure 5D). The temporal profile of Ca^{2+} signals reflected the structure of a cued reaching task, with the signal in many corticopontine neurons being tightly linked to the “go” cue (Figures 5E and 5F) (Li et al., 2015). Repeated recordings from identified neurons were possible both across trials within a session early in the expression time course (Figures 5E and 5F) and across many behavioral sessions for over 2 months post-infection. Thus, rAAV2-retro confers the ability to express sensors in projection neurons at levels sufficient for imaging, creating many new opportunities for deciphering the contributions of specific projections to neural circuit computations.

Finally, we evaluated the utility of rAAV2-retro for delivery of effectors, such as the CRISPR/Cas9 gene editing system, to projection neurons (Figure 6) (Cong et al., 2013). Specifically, we

packaged into rAAV2-retro the *Staphylococcus aureus* Cas9 (SaCas9; Slaymaker et al., 2016) and a single guide RNA (sgRNA) designed to ablate the expression of tdTomato (Experimental Procedures). Delivery of rAAV2-retro-SaCas9-anti-tdTomato to the BPN of animals expressing tdTomato in cortical layer V excitatory neurons resulted in suppression of tdTomato expression in $88.6\% \pm 0.7\%$ of SaCas9-expressing layer V neurons (Figure 6B, bottom panel, and Figure 6C; $n = 3$). In contrast, delivery of a non-targeted SaCas9 did not lead to any discernible changes, with only $4.4\% \pm 3.2\%$ of cells displaying potential reduction in tdTomato expression (Figure 6B, top panel, and Figure 6C; $n = 3$). Furthermore, tdTomato expression remained unaffected in layer V neurons that were inaccessible via pontine injection. The rAAV2-retro system thus permits efficient gene modification selectively in neurons projecting to specific areas of interest.

Collectively, these observations establish rAAV2-retro as an effective reagent to genetically access projection neurons for functional interrogation of neural circuits and, in the long run, for possible therapeutics.

DISCUSSION

Recombinant adeno-associated viruses (rAAVs) can greatly facilitate the functional dissection of mammalian neural circuits and hold promise for therapeutic intervention in disorders of the nervous system. We have used directed evolution to endow the AAV capsid with the additional capacity for efficient retrograde access to projection neurons in many neural circuits. The newly engineered rAAV2-retro offers up to two orders of magnitude enhancement in retrograde transport compared to commonly used AAV serotypes, matching the efficacy of synthetic retrograde tracers in many circuits. The level of transgene expression achieved with rAAV2-retro via retrograde access is ample for interrogating neural circuit function, as well as for targeted manipulations of the neuronal genome. Thus, by enabling selective monitoring and manipulation of projection neurons connecting different brain areas, rAAV2-retro-based tools are poised to provide insights into how large-scale networks enable brain function, and may form the basis for future therapeutic intervention in diseases characterized by progressive large-scale network dysfunction.

The markedly increased efficacy of retrograde access afforded by rAAV2-retro compared to its parental serotype AAV2 might have been enabled through an insertion-mediated disruption of the native binding site for heparin and/or through the creation of a new binding surface that incorporates the inserted peptide. This variant does have reduced heparin affinity (Figure S4), which could decrease virus sequestration in the extracellular matrix of the synaptic cleft and enhance local vector spread, as has been observed with rAAV1 and rAAV6 (Arnett et al., 2013). However, the resulting increase in vector spread alone cannot explain the efficacy of retrograde transport, as other inserted 7-mer sequences disrupt heparin binding similarly but do not affect retrograde transport (Dalkara et al., 2013). Furthermore, rAAV5 and rAAV9 do not bind heparin, yet their retrograde transport efficiency is similar to that of rAAV2. In support of the alternative explanation, the peptide insertions selected in the original selection (LAxxDxTKxA/LAxDxTKxxA)

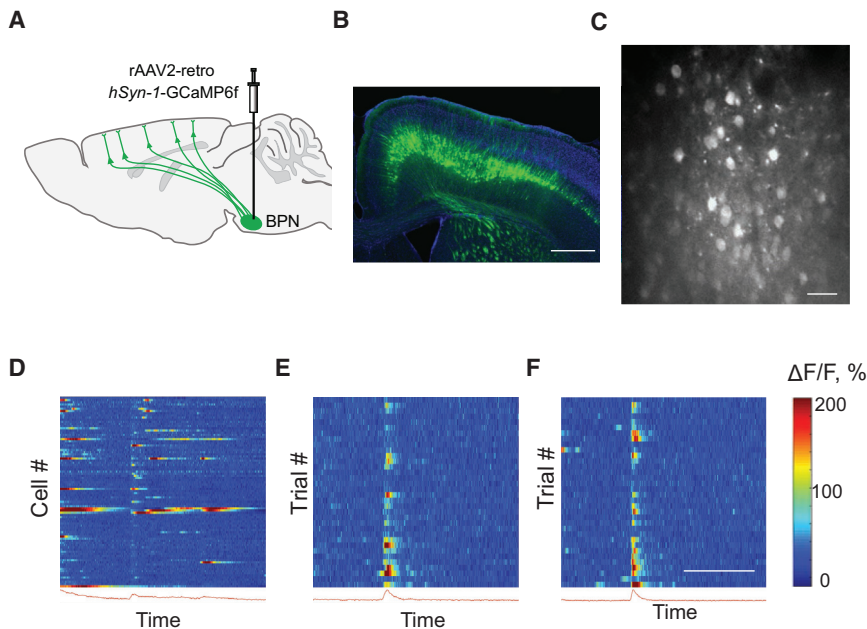


Figure 5. rAAV2-retro Supports Sufficient Transgene Expression for Functional Circuit Interrogation

(A) Schematic of the experiment. Expression of calcium indicator GCaMP6f is restricted to corticopontine neurons using localized injection of rAAV2-retro into the BPN.

(B) Cross-section of the mouse brain showing GCaMP6f expression throughout the corticopontine tract. Scale bar, 50 μ m.

(C) Maximum projection of an in vivo two-photon calcium image taken during a single reach showing layer V pyramidal tract somas and apical dendrites. Scale bar, 50 μ m.

(D) Activity of 89 ROIs during a single paw reach repetition (broken line denotes the tone “go” signal).

(E and F) Two examples of single corticopontine neurons, Neuron i (E) and Neuron ii (F), during 40 consecutive trials (same animal as in B–D). Scale bar, 4 s.

share the same overall composition, differing simply in the register of the conserved motif. The engineered peptide insertion might support enhanced binding to an existing cellular co-factor in the AAV pathway (e.g., the recently identified common AAV receptor; Pillay et al., 2016), or it might create a novel interaction with the cellular machinery, such as a cell-surface receptor and/or a component of the vesicular trafficking or nuclear entry pathway. Further experiments will be required to elucidate the mechanism of the profound enhancement in the efficacy of retrograde transport.

Despite the multiple orders of magnitude improvement in retrograde transport that rAAV2-retro offers over existing serotypes, a small set of projection neuron classes appears refractory to efficient retrograde infection by this newly evolved rAAV variant (Table S2). It should be noted, however, that other AAV serotypes fail to label these projections as well. Whether the expression level of the critical cellular factor that interfaces with this novel AAV variant in these neurons is extremely low—a conclusion supported for the corticothalamic and corticocollicular projections, for instance, by the observation that rAAV2-retro could still deliver sufficient Cre recombinase to cell bodies to direct a high level of expression for locally delivered Cre-dependent payloads (Table S2, highlighted entries)—or whether the factor is missing entirely remains to be determined in each case. Other viral reagents with retrograde functionality (such as HSV1; Enquist et al., 1998; or Hi-Ret lentivirus; Kato et al., 2011) might prove useful for targeting some of these projection neuron classes. Alternatively, additional AAV capsid engineering could extend retrograde transduction to all neurons.

Since gaining access to individual classes of projection neurons will be a critical enabling step in elucidating how local circuit dynamics and large-scale network function are coordinated, the rAAV2-retro vector system provides an important addition to the genetic toolkit for dissecting neural circuit function. Local circuit

computations are increasingly thought to depend on the dynamics of the entire neuronal population within a particular local circuit module (Fusi et al., 2016). How these dynamics map onto the different classes of projection neurons—and thus what information is passed on to the different downstream targets—remains unresolved for most circuits. rAAV2-retro-based vectors, alone or in combination with specific Cre transgenic lines, permit genetic access to specific populations of projections neurons. In turn, rAAV2-retro carrying rabies G glycoprotein can be used to trans-complement conditional rabies vectors (e.g., the newly developed, less toxic version described by Reardon et al., 2016) for access to presynaptic microcircuits impinging on particular classes of projection neurons (Brown and Hestrin, 2009). The resulting ability to selectively monitor and manipulate activity of individual projection neuron classes and their local microcircuits should provide insight into how projection neurons translate local circuit dynamics for their respective large-scale networks.

rAAV2-retro also holds promise for therapeutic intervention, with several possible applications. For example, in situations where pathology impacts large volumes of neural tissue, such as Alzheimer’s or lysosomal storage diseases, multiple injections pose a safety risk and may be insufficient to achieve the needed levels of transduction. However, a small number of injections in strategic locations can enable vector dispersal over large volumes (e.g., the corticopontine tract from the point of convergence in the BPN) or difficult-to-access tissue (e.g., spinal motor neurons from the muscle; Kaspar et al., 2003). Furthermore, large-scale functional networks have been implicated in the spread of many neurodegenerative disorders from their spatially localized onset. A prominent emerging view posits that deposition of abnormal protein assemblies in vulnerable neuronal populations triggers a pathological cascade of aberrant neuronal activity within, and disintegration of, large-scale functional

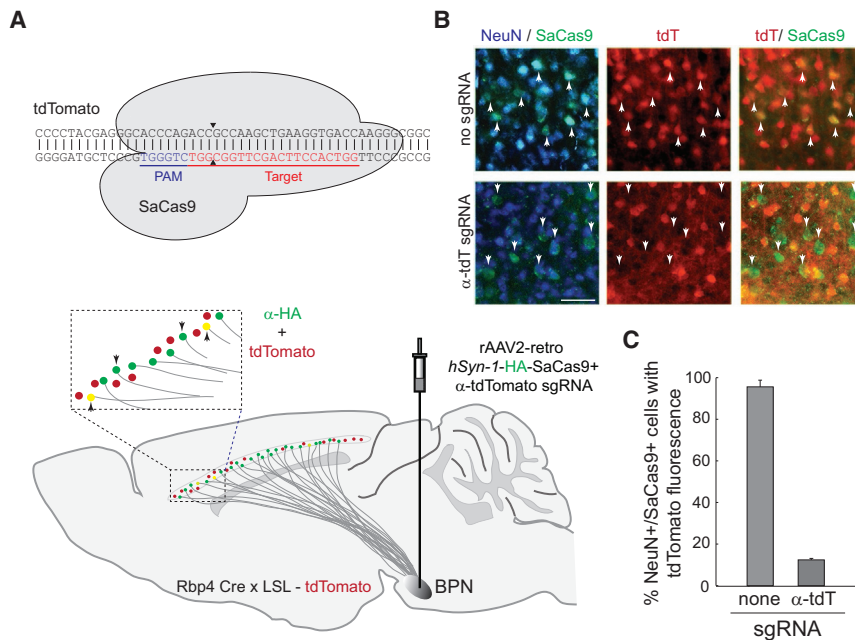


Figure 6. rAAV2-retro System Enables In Vivo Genome Editing Using CRISPR/Cas9

(A) Schematic of the experiment. Top panel: the rAAV2-retro system was used to deliver *Staphylococcus aureus* Cas9 (SaCas9) sgRNA combination engineered to ablate expression of tdTomato. Bottom panel: rAAV2-retro carrying the SaCas9-anti-tdTomato payload was injected into the BPN of mice expressing tdTomato from a single genomic locus in layer V neurons. SaCas9 was epitope tagged, permitting identification of retrogradely labeled neurons (green channel). Downward arrows: expected labeling following successful ablation of tdTomato. Upward arrows: expected labeling if tdTomato expression is unaffected.

(B) Representative images from brain sections of animals that received the CRISPR/Cas9 system targeted against tdTomato or carrying a non-targeted guide. tdT, tdTomato. Scale bar, 50 μ m.

(C) Efficiency of ablation. Error bars represent the SEM.

networks, ultimately leading to failure of neurological functions (for a recent review, see [Brettschneider et al., 2015](#)). Intriguingly, the affected neural networks appear capable of transiently overcoming the aberrant dynamics early in the disease, as patients with many neurodegenerative diseases often display periods of dramatic improvement. Thus, early intervention aimed at slowing down the spread of aggregates from the cortical origin of pathology might be sufficient to stabilize, or even restore, cognitive function. From this perspective, subcortically projecting neurons in the mesocortical regions where pathological protein aggregates first appear, in both Alzheimer's ([Braak and Braak, 1996](#)) and Parkinson's ([Braak et al., 2003](#)) disorders, constitute an attractive intervention target. Accessing those projection neurons with rAAV2-retro-based tools designed, for instance, to introduce a mutation that is capable of arresting further aggregation *in cis* ([Gregoire et al., 2014](#)) or to deliver chaperones capable of disassembling the aggregates ([Jackrel et al., 2014](#)) thus has the potential to slow down the progression of the most debilitating cognitive symptoms. Evaluating the efficiency and long-term safety of rAAV2-retro reagents in non-human primates will pave the path to their eventual consideration for these, and other, gene therapy approaches.

EXPERIMENTAL PROCEDURES

All procedures were in accordance with protocols approved by the Janelia Research Campus and the University of California, Berkeley Institutional Animal Care and Use Committees.

Library Generation and Viral Production

Four previously generated virus libraries were used at the start of the directed evolution procedure: (1) a random mutagenesis library, generated by subjecting the AAV2 *cap* gene (encoding virus proteins VP1-3 and assembly-activating protein, AAP) to error-prone PCR ([Maheshri et al., 2006](#)); (2) library of AAV2 *cap* gene variants containing 7-mer randomized peptide within a

10-mer insert of the form LAXXXXXXA between N587 and R588 ([Müller et al., 2003](#)); (3) library of AAV2 *cap* gene variants containing randomized loop regions ([Koerber et al., 2009](#)); and (4) a DNA shuffling library generated from wild-type AAV1, AAV2, AAV4, AAV5, AAV6, AAV8, and AAV9 *cap* gene sequences ([Koerber et al., 2008](#)). Each pool of mutant DNA had been originally sub-cloned into the replication-competent AAV packaging plasmid to create a viral plasmid library that, when packaged into AAV virions, can be selected for any new property or function. The replication-competent AAV system incorporates the mutant *cap* gene into the viral payload, and thus the genotype of each variant is linked to its phenotype. Capsid sequences of the desired property can then be recovered by DNA sequence analysis of the encapsulated AAV genome.

The four replication-competent AAV libraries were packaged by calcium phosphate transient transfection of HEK293T cells followed by virus harvest, iodixanol gradient centrifugation, and Amicon filtration ([Maheshri et al., 2006](#)).

In Vivo Virus or Tracer Injections

For virus injections, ~50–100 nL (mice) or ~250–500 nL (rats) virus-containing solution was slowly injected at each depth into the tissue. For tracer injections, 50 nL 5% Fluoro-Gold (Fluorochrome) in 0.9% NaCl, or 100 nL retrobeads (LumaFluor) diluted 1:1 in 0.9% NaCl, was injected at the same set of sites for each injection target.

Library Selection and Evolution

The four mutant virus libraries were pooled and injected either into the SNr or into the cerebellum of adult (6- to 8-week-old) wild-type C57/Bl6J mice (either sex; Charles River). Three weeks following injections, striatal or hindbrain tissue was accordingly removed, DNA was extracted, and virions that had successfully reached the remote retrograde target tissue were PCR amplified and recloned into an rAAV packaging plasmid to create a new replication-competent AAV library for the next round of selection. After three selection steps, the rescued *cap* genes were randomly mutated by error-prone PCR using 5'-ACGCGGAAGCTTCGATCAACTACGCAG-3' and 5'-AGACCAAAGTTCAA CTGAACGAATTAACGG-3' as forward and reverse primers, respectively. Two additional *in vivo* selection rounds were then performed. Individual isolates were sequenced after rounds four and five to evaluate the degree of library enrichment ([Table S1](#)). Seventeen variants were chosen for secondary screening at the end of round five, and the corresponding *cap* gene sequences

were re-cloned into an rAAV helper plasmid. Individual high-titer preps of the parental wild-type AAV2 and of each of the seventeen chosen mutant variants carrying a CMV-EGFP payload were then performed by Vector BioLabs, Inc. The CMV promoter is typically weak in neurons, and thus this secondary screen provided a stringent test of the efficiency of retrograde transport. The individual AAV variants were injected either into the cerebellum or into the globus pallidus. After 3 weeks, endogenous, unamplified EGFP fluorescence was visualized in the regions expected to be labeled if retrograde transport was efficient. Mutant r5H6 (insert **LADQDYTKTA** + V708I + N382D) displayed the strongest retrograde transport in both circuits, and was thus chosen for further analysis and named rAAV2-retro (see [Supplemental Information](#) for the complete gene sequence).

Payloads and Promoters Used in the Study

For all subsequent experiments, the CMV promoter was replaced with a promoter known to be more robust in adult neurons. Cre recombinase and the GCaMP6f calcium sensor were driven by the human *Synapsin-1* (*hSyn1*) promoter, all of the fluorophores were driven by the CAG promoter, and the color-flipping construct was driven by the *EF1 α* promoter.

Virus Production for the Quantification of Retrograde Efficiency

hSyn-Cre payload was packaged using rAAV1, rAAV2, rAAV5, rAAV8, rAAV9, DJ, and rAAV2-retro capsids at the Janelia Virus Shared Resource. All seven virus preparations were processed in parallel and were titer matched before in vivo injections. All lots were diluted to the lowest measured titer (1.3E12 GC/mL), and each virus was injected into the right pontine nucleus of three to five adult *Rosa26-Lox-STOP-Lox-H2B-EGFP* mice (He et al., 2012).

Histology

Animals were sacrificed 2–3 weeks following virus injections, at which point the brains were harvested and the right hemisphere was sagittally sectioned at a thickness of 50 μ m. In the triple-labeling experiment in [Figure 1B](#) and [Movie S1](#), the fluorophores were antibody amplified; otherwise, unstained sections were used. The sections were mounted in VECTASHIELD Antifade Mounting Medium containing DAPI (Vector Laboratories) and imaged using a P-E Panoramic slide scanner (3D Histech) using a 20 \times objective and FITC and DAPI filters.

Retrograde Transport Quantification

To quantify retrograde transport, the extent of corticopontine labeling was assessed in sagittal sections lateral to the injection tract (\sim 1 mm lateral with respect to midline) taken from *Rosa26-Lox-STOP-Lox-H2B-EGFP* animals injected in the basal pons with various AAV serotypes carrying a Cre recombinase transgene. Images obtained with the Panoramic slide scanner were stitched together and then analyzed using custom software written in MATLAB (MathWorks) to detect the GFP-labeled nuclei across the cortex.

For each chosen sagittal section, a region of interest (ROI) was manually drawn around the cortex to isolate the area in the image for automated cell counting. To enhance the detection of nuclei, the image was then convolved with a “Mexican Hat” kernel comprising the difference of two Gaussians (26.00 μ m variance and 3.25 μ m variance). Image noise was reduced using a median filter, and peak detection was then performed. Linear density was computed as the number of labeled nuclei per mm of the total length of a line drawn manually to trace the outline of cortical layer V.

Quantification of Infection Efficiency at the Injection Site

For rAAV2, rAAV9, and rAAV2-retro, additional analysis of infection efficiency at the injection site was performed. A single sagittal section spanning the middle of the injection site—as judged by the presence of extensive labeling along the injection tract—was chosen for each of the injected brains. The green channel was convolved with the “Mexican Hat” kernel (see above), and peaks were then detected as local maxima on these threshold images using custom functions written in MATLAB. An ROI was drawn over the midbrain area containing the BPN but excluding the injection tract, and the total number of labeled nuclei within the ROI was tabulated.

Analysis of the Generality of Retrograde Transport

Rosa26-Lox-STOP-Lox-H2B-EGFP mice were injected with 25 nL rAAV2-retro *hSyn1-Cre* (1.3E12 GC/mL) in the dorsal striatum. Three weeks after injection, coronally sectioned brains were imaged using a Panoramic scanner to visualize DAPI-stained nuclei and green fluorescence from H2B-GFP-expressing nuclei. The green channel was similarly used for the detection of labeled nuclei (see above). The blue channel of each section was aligned to the Nissl images from the Allen Brain Institute’s standardized mouse brain atlas using custom analysis routines written with the help of the MATLAB Image Processing Toolbox. The annotated regions from the Allen Brain Institute’s mouse brain atlas were then used to assign detected neurons in aligned sections to specific brain regions (Kuan et al., 2015).

We note that finite precision of the reference atlas, together with anatomical variability of individual brains, limits the robustness of this semi-automated process to prominent afferent inputs.

Imaging of Neuronal Population Activity In Vivo following Retrograde Delivery of GCaMP6f

Seven adult mice were implanted with custom-made headposts as previously described (Osborne and Dudman, 2014). rAAV2-retro carrying an *hSyn1-GCaMP6f* (1.0E13 GC/mL) payload was injected into the BPN using a Nanoliter 2010 injector (World Precision Instruments). A cranial window was placed over the primary motor cortex. All animals had visually identifiable GCaMP6f-expressing cells in layer V of M1 1 week post-injection. Then the animals were habituated to head fixation in a custom-built apparatus and trained to retrieve a food pellet as previously described (Guo et al., 2015). Calcium transients during behavior were imaged by exciting GCaMP6f at 920 nm. Emission light passed through a 565 DCXR dichroic filter (Chroma Technology) and an ET525/50 m-2p filter (Chroma Technology) and was detected by a GaAsP photomultiplier tube (10770PB-40, Hamamatsu). Images (512 \times 512 pixels) were acquired at \sim 30 Hz with resonating scanners using ScanImage software.

CRISPR/Cas9 Genome Editing

The CMV promoter in pAAV-CMV-SaCas9-empty (Slaymaker et al., 2016) was replaced with *hSyn1* to generate pAAV-*hSyn1*-SaCas9-empty. Oligonucleotides encoding sgRNA protospacer sequences were custom ordered, phosphorylated, hybridized, and ligated into the *Bsa*I restriction sites of pAAV-*hSyn1*-SaCas9-empty to generate pAAV-*hSyn1*-SaCas9-anti-tdTomato-1 to 10 (see [Supplemental Information](#) for oligonucleotide sequences tested and details of the in vitro selection procedure). sgRNA 7, one of two that appeared to direct two cleavage events within the tdTomato sequence in vitro, was packaged into rAAV2-retro and used for in vivo genome editing.

Approximately 100 nL rAAV2-retro-*hSyn1*-SaCas9-anti-tdTomato (5.0 E13 GC/mL) or rAAV2-retro-*hSyn1*-SaCas9-empty was then injected into the BPN of *Rbp4_KL100 Cre* \times tdTomato mice as described above. Six weeks after injections, brains were harvested and 40 μ m thick coronal sections were cut, stained against the HA-tagged Cas9, and imaged using a Zeiss Axio Observer A1 inverted microscope. Quantification of immunostaining was performed using ImageJ analysis software (NIH).

ACCESSION NUMBERS

The accession number for the AAV2-retro *cap* gene sequence reported in this paper is GenBank: KX904530.

SUPPLEMENTAL INFORMATION

Supplemental Information includes Supplemental Experimental Procedures, four figures, two tables, and one movie and can be found with this article online at <http://dx.doi.org/10.1016/j.neuron.2016.09.021>.

A video abstract is available at <http://dx.doi.org/10.1016/j.neuron.2016.09.021#mmc4>.

AUTHOR CONTRIBUTIONS

L.L.L., D.V.S., and A.Y.K. conceived the project; D.G.R.T., B.-Y.H., J.T.D., A.W.H., L.L.L., D.V.S., and A.Y.K. designed and oversaw the molecular

evolution process; B.-Y.H. performed library packaging, amplifications, and sequencing; K.D.R. designed and oversaw viral production and quality control process; D.G.R.T., S.V., T.G., M.L., S.L., S.M., E.K., D.O., and C.-C.H. performed experiments; D.G.R.T. wrote custom analysis code; D.G.R.T., S.V., T.G., and D.O. analyzed the data; and D.G.R.T., L.L.L., D.V.S., and A.Y.K. wrote the manuscript. C.R.G. and J.S. provided essential reagents, expertise, and input to the manuscript.

ACKNOWLEDGMENTS

We are indebted to K. Svoboda for suggesting the use of *Rosa26-STOP-Lox-H2B-EGFP* mice. We thank H. Adesnik for providing the *Rbp4_KL 100 Cre* × *tdTomato* mouse line, J. Brousseau for invaluable assistance with the pilot experiments, M. Proskurin for help with the rat experiments, and J. Santiago-Ortiz for help with the CRISPR/Cas9 experiments. We are grateful to the members of the J.T.D., A.W.H., Jessell, Ji, A.Y.K., Petreanu, Sabatini, Spruston, Svoboda, and Zuker labs for beta testing rAAV2-retro and contributing their findings to the knowledge base summarized in Table S2. T. Jessell, N. Spruston, and K. Svoboda offered useful discussions and comments on the manuscript. D.V.S. is supported by NIH R01EY022975 and T.G. by F32GM113446. This work was supported by the Howard Hughes Medical Institute.

Received: June 5, 2016

Revised: August 26, 2016

Accepted: September 9, 2016

Published: October 6, 2016

REFERENCES

- Amett, A.L., Beutler, L.R., Quintana, A., Allen, J., Finn, E., Palmiter, R.D., and Chamberlain, J.S. (2013). Heparin-binding correlates with increased efficiency of AAV1- and AAV6-mediated transduction of striated muscle, but negatively impacts CNS transduction. *Gene Ther.* *20*, 497–503.
- Baer, G.M., Shanthaveerappa, T.R., and Bourne, G.H. (1965). Studies on the pathogenesis of fixed rabies virus in rats. *Bull. World Health Organ.* *33*, 783–794.
- Braak, H., and Braak, E. (1996). Development of Alzheimer-related neurofibrillary changes in the neocortex inversely recapitulates cortical myelogenesis. *Acta Neuropathol.* *92*, 197–201.
- Braak, H., Rüb, U., Gai, W.P., and Del Tredici, K. (2003). Idiopathic Parkinson's disease: possible routes by which vulnerable neuronal types may be subject to neuroinvasion by an unknown pathogen. *J Neural Transm (Vienna)* *110*, 517–536.
- Brettschneider, J., Del Tredici, K., Lee, V.M.-Y., and Trojanowski, J.Q. (2015). Spreading of pathology in neurodegenerative diseases: a focus on human studies. *Nat. Rev. Neurosci.* *16*, 109–120.
- Brodal, P., and Bjaalie, J.G. (1992). Organization of the pontine nuclei. *Neurosci. Res.* *13*, 83–118.
- Brown, S.P., and Hestrin, S. (2009). Intracortical circuits of pyramidal neurons reflect their long-range axonal targets. *Nature* *457*, 1133–1136.
- Callaway, E.M., and Luo, L. (2015). Monosynaptic circuit tracing with glycoprotein-deleted rabies viruses. *J. Neurosci.* *35*, 8979–8985.
- Castle, M.J., Gershenson, Z.T., Giles, A.R., Holzbaier, E.L., and Wolfe, J.H. (2014). Adeno-associated virus serotypes 1, 8, and 9 share conserved mechanisms for anterograde and retrograde axonal transport. *Hum. Gene Ther.* *25*, 705–720.
- Chen, T.-W., Wardill, T.J., Sun, Y., Pulver, S.R., Renninger, S.L., Baohan, A., Schreiter, E.R., Kerr, R.A., Orger, M.B., Jayaraman, V., et al. (2013). Ultrasensitive fluorescent proteins for imaging neuronal activity. *Nature* *499*, 295–300.
- Cong, L., Ran, F.A., Cox, D., Lin, S., Barretto, R., Habib, N., Hsu, P.D., Wu, X., Jiang, W., Marraffini, L.A., and Zhang, F. (2013). Multiplex genome engineering using CRISPR/Cas systems. *Science* *339*, 819–823.
- Coulon, P., Derbin, C., Kucera, P., Lafay, F., Prehaud, C., and Flamand, A. (1989). Invasion of the peripheral nervous systems of adult mice by the CVS strain of rabies virus and its avirulent derivative AvO1. *J. Virol.* *63*, 3550–3554.
- Dalkara, D., Byrne, L.C., Klimczak, R.R., Visel, M., Yin, L., Merigan, W.H., Flannery, J.G., and Schaffer, D.V. (2013). In vivo-directed evolution of a new adeno-associated virus for therapeutic outer retinal gene delivery from the vitreous. *Sci. Transl. Med.* *5*, 189ra76.
- Enquist, L.W., Husak, P.J., Banfield, B.W., and Smith, G.A. (1998). Infection and spread of alphaherpesviruses in the nervous system. *Adv. Virus Res.* *51*, 237–347.
- Fusi, S., Miller, E.K., and Rigotti, M. (2016). Why neurons mix: high dimensionality for higher cognition. *Curr. Opin. Neurobiol.* *37*, 66–74.
- Gaudet, D., de Wal, J., Tremblay, K., Déry, S., van Deventer, S., Freidig, A., Brisson, D., and Méthot, J. (2010). Review of the clinical development of alipogene tiparvec gene therapy for lipoprotein lipase deficiency. *Atheroscler. Suppl.* *11*, 55–60.
- Gerfen, C.R. (1989). The neostriatal mosaic: striatal patch-matrix organization is related to cortical lamination. *Science* *246*, 385–388.
- Gerfen, C.R., Paletzki, R., and Heintz, N. (2013). GENSAT BAC cre-recombinase driver lines to study the functional organization of cerebral cortical and basal ganglia circuits. *Neuron* *80*, 1368–1383.
- Gregoire, S., Zhang, S., Costanzo, J., Wilson, K., Fernandez, E.J., and Kwon, I. (2014). Cis-suppression to arrest protein aggregation in mammalian cells. *Biotechnol. Bioeng.* *111*, 462–474.
- Guo, J.L., and Lee, V.M. (2014). Cell-to-cell transmission of pathogenic proteins in neurodegenerative diseases. *Nat. Med.* *20*, 130–138.
- Guo, J.-Z., Graves, A.R., Guo, W.W., Zheng, J., Lee, A., Rodríguez-González, J., Li, N., Macklin, J.J., Phillips, J.W., Mense, B.D., et al. (2015). Cortex commands the performance of skilled movement. *eLife* *4*, e10774.
- He, M., Liu, Y., Wang, X., Zhang, M.Q., Hannon, G.J., and Huang, Z.J. (2012). Cell-type-based analysis of microRNA profiles in the mouse brain. *Neuron* *73*, 35–48.
- Hollis, E.R., 2nd, Kadoya, K., Hirsch, M., Samulski, R.J., and Tuszynski, M.H. (2008). Efficient retrograde neuronal transduction utilizing self-complementary AAV1. *Mol. Ther.* *16*, 296–301.
- Jackrel, M.E., DeSantis, M.E., Martinez, B.A., Castellano, L.M., Stewart, R.M., Caldwell, K.A., Caldwell, G.A., and Shorter, J. (2014). Potentiated Hsp104 variants antagonize diverse proteotoxic misfolding events. *Cell* *156*, 170–182.
- Junyent, F., and Kremer, E.J. (2015). CAV-2—why a canine virus is a neurobiologist's best friend. *Curr. Opin. Pharmacol.* *24*, 86–93.
- Kaplitt, M.G., Feigin, A., Tang, C., Fitzsimons, H.L., Mattis, P., Lawlor, P.A., Bland, R.J., Young, D., Strybing, K., Eidelberg, D., and During, M.J. (2007). Safety and tolerability of gene therapy with an adeno-associated virus (AAV) borne GAD gene for Parkinson's disease: an open label, phase I trial. *Lancet* *369*, 2097–2105.
- Kaspar, B.K., Erickson, D., Schaffer, D., Hinh, L., Gage, F.H., and Peterson, D.A. (2002). Targeted retrograde gene delivery for neuronal protection. *Mol. Ther.* *5*, 50–56.
- Kaspar, B.K., Lladó, J., Sherkat, N., Rothstein, J.D., and Gage, F.H. (2003). Retrograde viral delivery of IGF-1 prolongs survival in a mouse ALS model. *Science* *301*, 839–842.
- Kato, S., Kobayashi, K., Inoue, K., Kuramochi, M., Okada, T., Yaginuma, H., Morimoto, K., Shimada, T., Takada, M., and Kobayashi, K. (2011). A lentiviral strategy for highly efficient retrograde gene transfer by pseudotyping with fusion envelope glycoprotein. *Hum. Gene Ther.* *22*, 197–206.
- Kelly, R.M., and Strick, P.L. (2000). Rabies as a transneuronal tracer of circuits in the central nervous system. *J. Neurosci. Methods* *103*, 63–71.
- Kern, A., Schmidt, K., Leder, C., Müller, O.J., Wobus, C.E., Bettinger, K., Von der Lieth, C.W., King, J.A., and Kleinschmidt, J.A. (2003). Identification of a heparin-binding motif on adeno-associated virus type 2 capsids. *J. Virol.* *77*, 11072–11081.

- Koerber, J.T., Maheshri, N., Kaspar, B.K., and Schaffer, D.V. (2006). Construction of diverse adeno-associated viral libraries for directed evolution of enhanced gene delivery vehicles. *Nat. Protoc.* *1*, 701–706.
- Koerber, J.T., Jang, J.-H., and Schaffer, D.V. (2008). DNA shuffling of adeno-associated virus yields functionally diverse viral progeny. *Mol. Ther.* *16*, 1703–1709.
- Koerber, J.T., Klimczak, R., Jang, J.-H., Dalkara, D., Flannery, J.G., and Schaffer, D.V. (2009). Molecular evolution of adeno-associated virus for enhanced glial gene delivery. *Mol. Ther.* *17*, 2088–2095.
- Kotterman, M.A., and Schaffer, D.V. (2014). Engineering adeno-associated viruses for clinical gene therapy. *Nat. Rev. Genet.* *15*, 445–451.
- Kremer, E.J., Boutin, S., Chillon, M., and Danos, O. (2000). Canine adenovirus vectors: an alternative for adenovirus-mediated gene transfer. *J. Virol.* *74*, 505–512.
- Kuan, L., Li, Y., Lau, C., Feng, D., Bernard, A., Sunkin, S.M., Zeng, H., Dang, C., Hawrylycz, M., and Ng, L. (2015). Neuroinformatics of the allen mouse brain connectivity atlas. *Methods* *73*, 4–17.
- Legg, C.R., Mercier, B., and Glickstein, M. (1989). Corticopontine projection in the rat: the distribution of labelled cortical cells after large injections of horseradish peroxidase in the pontine nuclei. *J. Comp. Neurol.* *286*, 427–441.
- Li, N., Chen, T.-W., Guo, Z.V., Gerfen, C.R., and Svoboda, K. (2015). A motor cortex circuit for motor planning and movement. *Nature* *519*, 51–56.
- Maheshri, N., Koerber, J.T., Kaspar, B.K., and Schaffer, D.V. (2006). Directed evolution of adeno-associated virus yields enhanced gene delivery vectors. *Nat. Biotechnol.* *24*, 198–204.
- Miller, M.W., and Vogt, B.A. (1984). Direct connections of rat visual cortex with sensory, motor, and association cortices. *J. Comp. Neurol.* *226*, 184–202.
- Müller, O.J., Kaul, F., Weitzman, M.D., Pasqualini, R., Arap, W., Kleinschmidt, J.A., and Trepel, M. (2003). Random peptide libraries displayed on adeno-associated virus to select for targeted gene therapy vectors. *Nat. Biotechnol.* *21*, 1040–1046.
- Muridharan, G., Samulski, R.J., and Asokan, A. (2014). Biology of adeno-associated viral vectors in the central nervous system. *Front. Mol. Neurosci.* *7*, 76.
- Nagy, A. (2000). Cre recombinase: the universal reagent for genome tailoring. *Genesis* *26*, 99–109.
- Ohka, S., Yang, W.-X., Terada, E., Iwasaki, K., and Nomoto, A. (1998). Retrograde transport of intact poliovirus through the axon via the fast transport system. *Virology* *250*, 67–75.
- Ojala, D.S., Amara, D.P., and Schaffer, D.V. (2015). Adeno-associated virus vectors and neurological gene therapy. *Neuroscientist* *21*, 84–98.
- Osborne, J.E., and Dudman, J.T. (2014). RIVETS: a mechanical system for in vivo and in vitro electrophysiology and imaging. *PLoS ONE* *9*, e89007.
- Pan, W.X., Mao, T., and Dudman, J.T. (2010). Inputs to the dorsal striatum of the mouse reflect the parallel circuit architecture of the forebrain. *Front. Neuroanat.* *4*, 147.
- Piersanti, S., Astrologo, L., Licursi, V., Costa, R., Roncaglia, E., Gennetier, A., Ibanes, S., Chillon, M., Negri, R., Tagliafico, E., et al. (2013). Differentiated neuroprogenitor cells incubated with human or canine adenovirus, or lentiviral vectors have distinct transcriptome profiles. *PLoS ONE* *8*, e69808.
- Pillay, S., Meyer, N.L., Puschnik, A.S., Davulcu, O., Diep, J., Ishikawa, Y., Jae, L.T., Wosen, J.E., Nagamine, C.M., Chapman, M.S., and Carette, J.E. (2016). An essential receptor for adeno-associated virus infection. *Nature* *530*, 108–112.
- Ramón y Cajal, S. (1911). *Histologie du Système Nerveux de l'homme et des Vertébrés* (Maloine).
- Reardon, T.R., Murray, A.J., Turi, G.F., Wirblich, C., Croce, K.R., Schnell, M.J., Jessell, T.M., and Losonczy, A. (2016). Rabies virus CVS-N2c(ΔG) strain enhances retrograde synaptic transfer and neuronal viability. *Neuron* *89*, 711–724.
- Rothermel, M., Brunert, D., Zabawa, C., Díaz-Quesada, M., and Wachowiak, M. (2013). Transgene expression in target-defined neuron populations mediated by retrograde infection with adeno-associated viral vectors. *J. Neurosci.* *33*, 15195–15206.
- Saunders, A., Johnson, C.A., and Sabatini, B.L. (2012). Novel recombinant adeno-associated viruses for Cre activated and inactivated transgene expression in neurons. *Front. Neural Circuits* *6*, 47.
- Schmued, L.C., and Fallon, J.H. (1986). Fluoro-Gold: a new fluorescent retrograde axonal tracer with numerous unique properties. *Brain Res.* *377*, 147–154.
- Schnell, M.J., McGettigan, J.P., Wirblich, C., and Papaneri, A. (2010). The cell biology of rabies virus: using stealth to reach the brain. *Nat. Rev. Microbiol.* *8*, 51–61.
- Seeley, W.W., Crawford, R.K., Zhou, J., Miller, B.L., and Greicius, M.D. (2009). Neurodegenerative diseases target large-scale human brain networks. *Neuron* *62*, 42–52.
- Simão, D., Pinto, C., Fernandes, P., Peddie, C.J., Piersanti, S., Collinson, L.M., Salinas, S., Saggio, I., Schiavo, G., Kremer, E.J., et al. (2016). Evaluation of helper-dependent canine adenovirus vectors in a 3D human CNS model. *Gene Ther.* *23*, 86–94.
- Slaymaker, I.M., Gao, L., Zetsche, B., Scott, D.A., Yan, W.X., and Zhang, F. (2016). Rationally engineered Cas9 nucleases with improved specificity. *Science* *351*, 84–88.
- Soudais, C., Laplace-Builhe, C., Kissa, K., and Kremer, E.J. (2001). Preferential transduction of neurons by canine adenovirus vectors and their efficient retrograde transport in vivo. *FASEB J.* *15*, 2283–2285.
- Taymans, J.-M., Vandenberghe, L.H., Haute, C.V.D., Thiry, I., Deroose, C.M., Mortelmans, L., Wilson, J.M., Debyser, Z., and Baekelandt, V. (2007). Comparative analysis of adeno-associated viral vector serotypes 1, 2, 5, 7, and 8 in mouse brain. *Hum. Gene Ther.* *18*, 195–206.
- Tomioka, R., Okamoto, K., Furuta, T., Fujiyama, F., Iwasato, T., Yanagawa, Y., Obata, K., Kaneko, T., and Tamamaki, N. (2005). Demonstration of long-range GABAergic connections distributed throughout the mouse neocortex. *Eur. J. Neurosci.* *21*, 1587–1600.
- Towne, C., Schneider, B.L., Kieran, D., Redmond, D.E., Jr., and Aebischer, P. (2010). Efficient transduction of non-human primate motor neurons after intramuscular delivery of recombinant AAV serotype 6. *Gene Ther.* *17*, 141–146.
- Ugolini, G., Kuypers, H.G., and Simmons, A. (1987). Retrograde transneuronal transfer of herpes simplex virus type 1 (HSV 1) from motoneurons. *Brain Res.* *422*, 242–256.
- Wickersham, I.R., Finke, S., Conzelmann, K.K., and Callaway, E.M. (2007). Retrograde neuronal tracing with a deletion-mutant rabies virus. *Nat. Methods* *4*, 47–49.

Neuron, Volume 92

Supplemental Information

A Designer AAV Variant Permits Efficient

Retrograde Access to Projection Neurons

D. Gowanlock R. Tervo, Bum-Yeol Hwang, Sarada Viswanathan, Thomas Gaj, Maria Lavzin, Kimberly D. Ritola, Sarah Lindo, Susan Michael, Elena Kuleshova, David Ojala, Cheng-Chiu Huang, Charles R. Gerfen, Jackie Schiller, Joshua T. Dudman, Adam W. Hantman, Loren L. Looger, David V. Schaffer, and Alla Y. Karpova

Supplemental Figure Legends

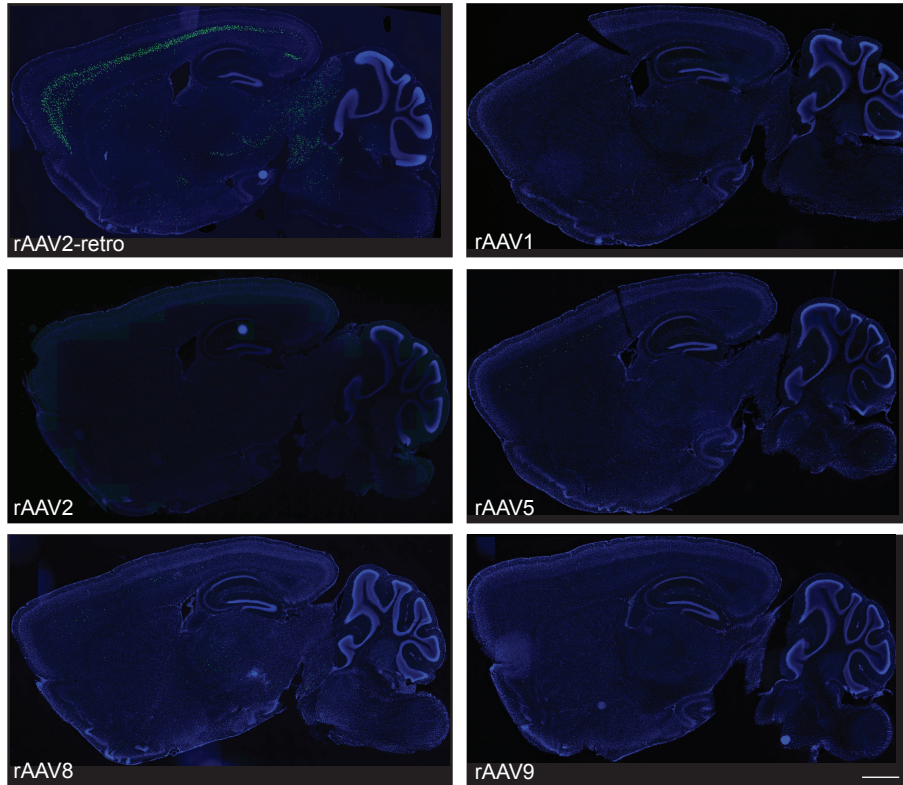
Figure S1, related to Figure 1. rAAV2-retro mediates efficient access to projection neurons in the rat. (A) Schematic of the example injection. Separate lots of rAAV2-retro expressing EGFP or tdTomato were injected in the striatum or superior colliculus, respectively, of an adult Long Evans rat. (B–E) Projection neurons in various brain regions labeled through these localized injections were imaged in coronal sections three weeks following virus delivery. Scale bars: 2 mm (B), 1 mm (E).

Figure S2, related to Figure 2. No naturally-occurring AAV serotypes match rAAV2-retro performance in corticopontine circuit. Representative images of corticopontine labeling in sagittal sections lateral to the injection tract (~1 mm lateral with respect to midline) taken from *Rosa26-Lox-STOP-Lox-H2B-EGFP* animals injected in the basal pons with various AAV serotypes carrying the Cre recombinase transgene. Scale bar: 1 mm.

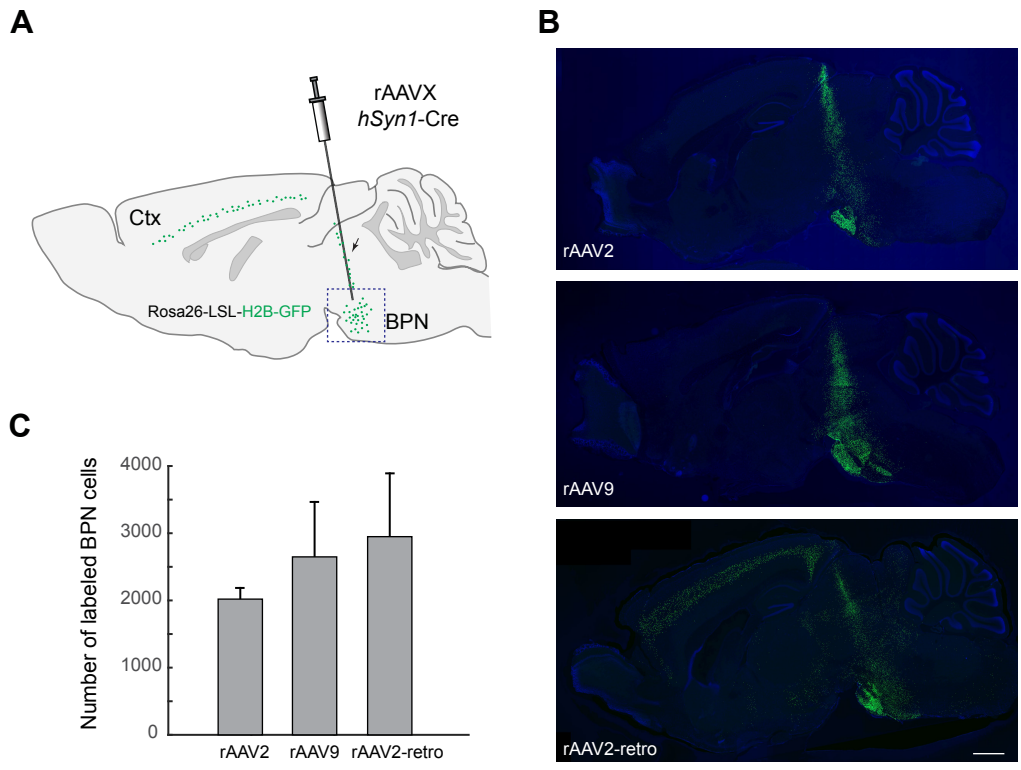
Figure S3, related to Figure 2. Differences in retrograde efficiency between rAAV2-retro and naturally occurring AAV serotypes cannot be explained by differences in functional titers. (A) Schematic of the analysis. Sagittal sections taken from *Rosa26-Lox-STOP-Lox-H2B-EGFP* animals injected in the basal pons with rAAV2, rAAV9 and rAAV2-retro carrying Cre recombinase that span the middle of the injection site were identified by the presence of an injection tract (arrow). The midbrain region around the basal pontine nuclei (BPN) was then used for the analysis. (B) Representative images of pontine labeling for rAAV2, rAAV9 and rAAV2-retro. Scale bar: 1 mm. (C) Quantification of infection efficiency at the injection site (see Experimental Procedures).

Figure S4, related to Figure 1. Reduced heparin affinity for rAAV2-retro compared to its parental serotype AAV2. (A) Schematic of the heparin binding assay. 10^{11} purified genomic particles were loaded onto a heparin column previously equilibrated with 150 mM NaCl and 50 mM Tris at pH 7.5. Elution was then performed by increasing the concentration of NaCl in steps of 50 mM. (B) Fraction of virus eluted with increasing concentrations of NaCl. To quantify the amount of eluted virus, a small fraction of each elution was used to infect HEK293T cells, and the percentage of GFP positive cells was quantified 48

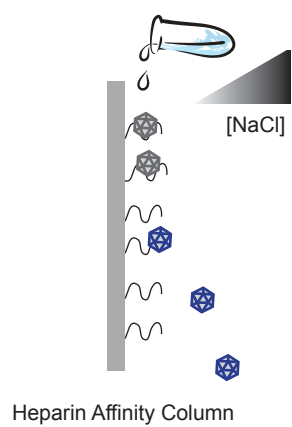
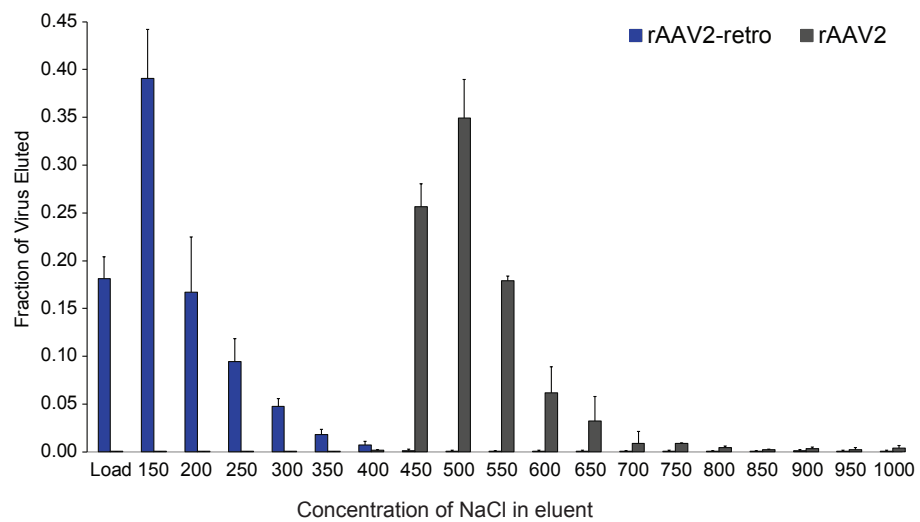
hours post-infection by flow cytometry. The load fraction represents the virus recovered in the column flow-through after sample loading in 150 mM NaCl. Error bars represent the S.D.



Tervo et al. Figure S2



Tervo et al. Figure S3

A**B**

Supplemental Tables

Table S1, related to Figure 1. Convergence of peptide insert sequences for variants isolated in rounds 4 and 5. Peptide insert sequences are listed in bold. Additional point mutations found in isolated variants are also listed. “x” indicates the presence of a mutation at a particular site when only a single specific substitution (e.g. N408S) was observed across different isolated variants. If, instead, the site was mutated in several variants, but a number of different substitutions were observed, the specific mutation for each variant was indicated by its single amino acid abbreviation (e.g. P, E, Y or D, for V182). The column of “other” substitutions lists point mutations found only in a single recovered variant.

Table S2, related to Figure 3. rAAV2-retro efficiency in various circuits. Qualitative estimate of the labeling efficiency, as reported by beta-testers. Low efficiency rather than absence of retrograde transport in corticothalamic and corticocollicular projections is suggested by efficient labeling of projection neurons following local delivery of high-copy number Cre-dependent payloads to projection neuron cell bodies (yellow rows).

Clone	loop	E36G	E67A	V182	S207G	N382D	N408S	T567A	Q598L	I648V	V708I	M235L	F284Y	S492	N496	other
4R-H-3	LAISDQTKHA										x					
4R-H-4	LAISDQTKHA						x				x				D	L59P
4R-H-5	LAKDQTKSTA						x				x					
4R-H-9	LANQDYTKTA														P	
4R-H-10	LAISDQTKHA										x				Y	
4R-H-12	LANQDYTKTA	x									x					
4R-H-15	LAISDQTKHA										x					
4R-H-16	LAHDITKNIA						x				x					
4R-H-17	LAHDITKNIA						x				x					
4R-SD-2	LAHDITKNIA		x		x		x				x					
4R-SD-3	LAHDITKNIA						x				x					
4R-SD-10	LAISDQTKHA						x				x					
4R-SD-11	LANQDYTKTA			E							x				P	
4R-SD-12	LAISDQTKHA					x					x					Q186R,D594N
4R-SD-15	LADQDYTKTA										x	x	x			
4R-SD-16	LAISDQTKHA			E			x				x					D69E
4R-SD-17	LAISDQTKHA			E							x				Y	
4R-SD-18	LAHDITKNIA						x				x					
5R-Hind1	LAQPDATKNA		x	I							x					
5R-Hind2	LAHDITKNIA		x		x						x					E12V,K137E
5R-Hind3	LANQDYTKTA		x								x					R585G,S662C
5R-Hind6	LADQDYTKTA					x					x					
5R-Hind8	LANQDYTKTA		x								x					
5R-Hind10	LADQDYTKTA	x					x				x					
5R-Hind11	LANQDYTKTA	x					x				x					N335K
5R-Hind12	LAHDITKNIA						x				x					
5R-Hind14	LAISDQTKHA										x					S423N
5R-Hind15	LAISDQTKHA										x					N214D
5R-Hind16	LAHDITKNIA						x				x					
5R-Hind17	LADQDYTKTA		x				x				x					
5R-Hind18	LAISDQTKHA										x					
5R-Hind19	LAHDITKNIA		x		x		x				x					H38L,E147A
5R-Hind22	LANQDYTKTA	x									x				P	N227D,N587S
5R-Hind23	LAHDITKNIA	x	x				x				x					
5R-Ce1	LANQDYTKTA		x								x				P	D41G,K105E,G163D
5R-Ce5	LADQDYTKTA						x				x					
5R-Ce6	LAQPDATKNA		x		x						x					P29A
5R-Ce8	LAKDQTKSTA										x					
5R-Ce9	LANQDYTKTA		x		x		x				x				P	

Tervo et al., Table S1

Injection location	Location of Projection Neurons	Labeling efficiency	Viral transgene	Mouse background
mouse mPFC (IL/PL)	MEC	strong	Cre	ROSA26-LSL-H2B-GFP
mouse mPFC (IL/PL)	LEC	strong	Cre	ROSA26-LSL-H2B-GFP
mouse mPFC (IL/PL)	contra mPFC	strong	Cre	ROSA26-LSL-H2B-GFP
mouse mPFC (IL/PL)	mediodorsal thalamus	moderate	Cre	ROSA26-LSL-H2B-GFP
mouse mPFC (IL/PL)	insular cortex	strong	Cre	ROSA26-LSL-H2B-GFP
mouse mPFC (IL/PL)	hippocampus- ventral CA1	strong	Cre	ROSA26-LSL-H2B-GFP
mouse mPFC (IL/PL)	AcG	strong	Cre	ROSA26-LSL-H2B-GFP
OFC	MEC	strong	Cre	ROSA26-LSL-H2B-GFP
OFC	LEC	Strong	Cre	ROSA26-LSL-H2B-GFP
OFC	contra OFC	strong	Cre	ROSA26-LSL-H2B-GFP
OFC	insular cortex	strong	Cre	ROSA26-LSL-H2B-GFP
OFC	hippocampus- ventral CA1	moderate	Cre	ROSA26-LSL-H2B-GFP
dorsal CA1	MEC	strong	Cre	ROSA26-LSL-H2B-GFP
dorsal CA2	LEC	strong	Cre	ROSA26-LSL-H2B-GFP
dorsal CA3	CA3	weak	Cre	ROSA26-LSL-H2B-GFP
dorsal CA4	nucleus reuniens of thalamus	weak	Cre	ROSA26-LSL-H2B-GFP
amygdala	mPFC	strong	Cre	ROSA26-LSL-H2B-GFP
lateral hypothalamus	mPFC	strong	Cre	ROSA26-LSL-H2B-GFP
dorsomedial striatum	mPFC	strong	Cre	ROSA26-LSL-H2B-GFP
NAcc	mPFC	strong	Cre	ROSA26-LSL-H2B-GFP
MEC	mPFC	moderate	FLPo	RCE:dual
mPFC	ventral CA1	moderate	FLPo	RCE:dual
mPFC	MEC	moderate	FLPo	RCE:dual
subiculum	nucleus accumbens	moderate	Cre	ROSA26-LSL-H2B-GFP
subiculum	ventral hippocampus	strong	Cre	ROSA26-LSL-H2B-GFP
subiculum	retrosplenial cortex	strong	Cre	ROSA26-LSL-H2B-GFP
subiculum	lateral entorhinal cortex	strong	Cre	ROSA26-LSL-H2B-GFP
subiculum	medial entorhinal cortex	strong	Cre	ROSA26-LSL-H2B-GFP
superior colliculus	layer 5 in visual cortex	very weak	GCaMP6s	wt
superior colliculus	layer 5 in visual cortex	very weak	Cre	Ai94
superior colliculus	layer 5 in visual cortex	strong	Cre	wt + in situ
AAV2/1-DIO-GCaMP6s				
dLGN	layer 6 in visual cortex	very weak	GCaMP6s	ROSA26-LSL-H2B-GFP
dLGN	layer 6 in visual cortex	very weak	Cre	Ai94
dLGN	layer 6 in visual cortex	strong	Cre	wt + in situ
AAV2/1-DIO-GCaMP6s				

Injection location	Location of Projection Neurons	Labeling efficiency	Viral transgene	Mouse background
visual cortex	contralateral visual cortex	strong	Cre	ROSA26-LSL-H2B-GFP
visual cortex	contralateral visual cortex	strong	GFP	wt
visual cortex	contralateral visual cortex	weak	GCaMP6s	wt
visual cortex	contralateral visual cortex	strong	tdTomato	wt
visual cortex	LGN	strong	tdTomato	wt
visual cortex	claustrum	strong	tdTomato	wt
visual cortex	cingulate	moderate	tdTomato	wt
visual cortex	LM	strong	tdTomato	wt
dorso-lateral striatum	M1	strong	tdTomato	wt
dorso-lateral striatum	M1	moderate	GFP	wt
dorso-lateral striatum	M2	strong	tdTomato	wt
dorso-lateral striatum	somatosensory cortex	strong	tdTomato	wt
dorso-lateral striatum	basolateral amygdala	strong	tdTomato	wt
dorso-lateral striatum	insular cortex	strong	tdTomato	wt
dorso-lateral striatum	entorhinal cortex	strong	tdTomato	wt
dorso-lateral striatum	Globus Pallidus	moderate	tdTomato	wt
dorso-lateral striatum	thalamus	moderate	tdTomato	wt
dorso-lateral striatum	intralaminar thalamic nuclei	strong	GFP	wt
dorso-lateral striatum	raphe nucleus	very weak	tdTomato	wt
dorso-lateral striatum	VTA	very weak	tdTomato	wt
basolateral amygdala	taste cortex	strong	DIO-tdTomato	Vglut-Cre
forelimb motor cortex	motor thalamus	weak	GFP	wt
nucleus tractus solitarius	lateral amygdala	moderate	tdTomato	wt
spinal cord	cortex	strong	DIO-tdTomato	Rbp4-Cre
spinal cord	cortex	strong	GFP	wt
spinal cord, lamina IX	spinal cord: presynaptic inhibitory neurons	strong	DIO-tdTomato	GAD2-Cre
muscle	spinal motor neurons	moderate	Cre	ROSA26-LSL-tdTomato
muscle	proprioceptor neurons	moderate	Cre	ROSA26-LSL-tdTomato

Tervo et al., Table S2

Full Experimental Procedures

All procedures were in accordance with protocols approved by the Janelia Research Campus and the University of California Berkeley Institutional Animal Care and Use Committees.

Library generation and viral production

Four previously generated virus libraries were used at the start of the directed evolution procedure: 1) a random mutagenesis library, generated by subjecting the AAV2 *cap* gene (encoding viral proteins VP1-3 and Assembly-activating protein, AAP) to error prone PCR (Maheshri et al., 2006); 2) a library of AAV2 *cap* gene variants containing 7-mer randomized peptide within a 10-mer insert of the form LAXXXXXXXXA between N587 and R588 (Müller et al., 2003); 3) a library of AAV2 *cap* gene variants containing randomized loop regions (Koerber et al., 2009), and 4) a DNA shuffling library generated from wild-type AAV1, AAV2, AAV4, AAV5, AAV6, AAV8 and AAV9 *cap* gene sequences (Koerber et al., 2008). Each pool of mutant DNA had been originally sub-cloned into the replication-competent AAV packaging plasmid to create a viral plasmid library that, when packaged into AAV virions, can be selected for any new property or function. The replication-competent AAV system incorporates the mutant *cap* gene into the viral payload, and thus the genotype of each variant is linked to its phenotype. Capsid sequences of the desired property can then be recovered by DNA sequence analysis of the encapsulated AAV genome.

The four replication-competent AAV libraries were packaged by calcium phosphate transient transfection of HEK293-T cells followed by virus harvest, iodixanol gradient centrifugation, and Amicon filtration (Maheshri et al., 2006).

***In vivo* virus or tracer injections**

For localized *in vivo* virus delivery, mice or rats were anaesthetized with isoflurane (~2% by volume in O₂; SurgiVet, Smiths Medical) and a small hole was drilled in the skull above the requisite injection site (see table below). For some injection sites, several injections were made at different depths (see table below). For viral injections, ~ 50–100 nl (mice) or 250–500 nl (rats) of virus containing solution was slowly injected at each depth into the tissue. For tracer injections, 50 nl of 5% Fluoro-Gold (Fluorochrome, Denver, CO) in 0.9% NaCl, or 100 nl of retro-beads (LumaFluor, Durham, NC) diluted 1:1 in 0.9% NaCl were injected at the same set of sites for each injection target. Injections were done with a pulled glass pipette (broken and beveled to 25–30 μm (outside diameter); Drummond Scientific,

Wiretrol II Capillary Microdispenser) back-filled with mineral oil. A fitted plunger was inserted into the pipette and advanced to displace the contents using a hydraulic manipulator (Narashige, MO-10). Retraction of the plunger was used to load the pipette with virus. The injection pipette was positioned with a Sutter MP-285 manipulator.

The following coordinates were used in this study:

Injection target	Injection coordinates, mm*
mouse substantia nigra pars reticulata	A/P: -3.5; M/L: 1.5; D/V: -4.0 and -4.5
mouse cerebellum	A/P: 7.1; M/L: 1.4; D/V: -0.8 and -0.5
mouse dorsomedial striatum	A/P: 0.6; M/L: 1.2; D/V -2.5
mouse dorsolateral striatum	A/P: 0.6; M/L: 2.25; D/V -2.6
mouse ventrolateral striatum	A/P: 0; M/L: 2.8; D/V -3.2
mouse pontine nucleus (BPN)	A/P: 0.40; M/L: 0.40; D/V: -5.50, -5.75, and -6.0
rat dorsomedial striatum	A/P 2.16; M/L 1.7 ; D/V -4.3
rat superior colliculus	A/P -6.0; M/L \pm 1.8; D/V -5.45

* All A/P coordinates are given with respect to Bregma; D/V coordinates are given with respect to the pia.

Library selection and evolution

The four mutant virus libraries were pooled and injected either into the substantia nigra pars reticulata or into the cerebellum of adult (6–8 week old) wild-type C57/Bl6J mice (either sex; Charles River). Three weeks after injection, striatal or hindbrain tissue was accordingly removed, DNA was extracted, and virions that had successfully reached the remote retrograde target tissue were PCR-amplified and recloned into rcAAV packaging plasmid to create a new replication competent AAV library for the next round of selection. After three selection steps, the rescued *cap* genes were randomly mutated by error prone PCR using 5'-ACGCGGAAGCTTCGATCAACTACGCAG-3' and 5'-AGACCAAAGTTCAACTGAAACGAATTAAACGG-3' as forward and reverse primers, respectively. Two additional *in vivo* selection rounds were then performed. Individual isolates were sequenced after rounds four and five to evaluate the degree of library enrichment (Table S1). Seventeen variants were chosen for secondary screening at the end of round five, and the corresponding *cap* gene sequences were recloned into an rAAV helper plasmid. Individual high-titer preps of the parental wild type AAV2 and of each of the seventeen chosen mutant variants carrying a *CMV-EGFP* payload were then performed by

Vector BioLabs, Inc (Philadelphia, PA). The *CMV* promoter is typically weak in neurons, and thus this secondary screen provided a stringent test of the efficiency of retrograde transport. The individual AAV variants were injected either into the cerebellum or into the globus pallidus. After three weeks, endogenous, unamplified EGFP fluorescence was visualized in the regions expected to be labeled if retrograde transport was efficient. Mutant r5H6 (insert **LADQDYTKTA** + V708I + N382D) displayed the strongest retrograde transport in both circuits, and was thus chosen for further analysis and named rAAV2-retro.

The full gene sequence of the selected variant is as follows (changes from the wild type AAV2 *cap* gene sequence are indicated in red):

```
ATGGCTGCCGATGGTTATCTTCCAGATTGGCTCGAGGACACTCTCTCTGAAGGAATAAGACAGTGGTG
GAAGCTCAAACCTGGCCCACCACCACAAAGCCCGCAGAGCGGCATAAGGACGACAGCAGGGGTCTT
GTGCTTCCTGGGTACAAGTACCTCGGACCCTTCAACGGACTCGACAAGGGAGAGCCGGTCAACGAGGC
AGACGCCGCGGCCCTCGAGCACGACAAAGCCTACGACCGGCAGCTCGACAGCGGAGACAACCCGTAC
CTCAAGTACAACCACGCCGACGCGGAGTTTCAGGAGCGCCTTAAAGAAGATACGTCTTTTGGGGGCAA
CCTCGGACGAGCAGTCTTCCAGGCGAAAAGAGGGTTCTTGAACCTCTGGGCCTGGTTGAGGAACCTG
TTAAGACGGCTCCGGGAAAAAGAGGCCGGTAGAGCACTCTCCTGTGGAGCCAGACTCCTCCTCGGG
AACCGGAAAGGCGGGCCAGCAGCCTGCAAGAAAAAGATTGAATTTTGGTCAGACTGGAGACGCAGAC
TCAGTACCTGACCCCCAGCCTCTCGGACAGCCACCAGCAGCCCCCTCTGGTCTGGGAACATAACGAT
GGCTACAGGCAGTGGCGCACCAATGGCAGACAATAACGAGGGCGCCGACGGAGTGGGTAATTCCTCG
GGAAATTGGCATTGCGATTCCACATGGATGGGCGACAGAGTCATCACCACCAGCACCCGAACCTGGGC
CCTGCCACCTACAACAACCACCTCTACAACAAATTTCCAGCCAATCAGGAGCCTCGAACGACAATC
ACTACTTTGGCTACAGCACCCCTTGGGGGTATTTTGACTTCAACAGATTCCACTGCCACTTTTCACCAC
GTGACTGGCAAAGACTCATCAACAACAACCTGGGGATTCCGACCCAAGAGACTCAACTTCAAGCTCTTT
AACATTCAAGTCAAAGAGGTACGCAGAATGACGGTACGACGACGATTGCCAATAACCTTACCAGCA
CGGTTCAAGTGTTTACTGACTCGGAGTACCAGCTCCCGTACGTCTCGGCTCGGCGCATCAAGGATGC
CTCCCGCGTTCCAGCAGACGTCTTCATGGTGCCACAGTATGGATACCTCACCTGAACGACGGGAG
TCAGGCAGTAGGACGCTCTTCAATTTTACTGCCTGGAGTACTTTCCTTCTCAGATGCTGCGTACCGGAAA
CAACTTTACCTTACGCTACACTTTTGAGGACGTTCCCTTTCCACAGCAGCTACGCTCACAGCCAGAGTCT
GGACCGTCTCATGAATCCTCTCATCGACCAGTACCTGTATTACTTGAGCAGAACAACACTCCAAGTG
GAACCACCACGCAGTCAAGGCTTCAGTTTTTCTCAGGCCGGAGCGAGTGACATTCGGGACCAGTCTAGG
AACTGGCTTCTGGACCCTGTTACCGCCAGCAGCGAGTATCAAAGACATCTGCGGATAACAACAACAG
TGAATACTCGTGGACTGGAGCTACCAAGTACCACCTCAATGGCAGAGACTCTCTGGTGAATCCGGGCC
CGGCCATGGCAAGCCACAAGGACGATGAAGAAAAGTTTTTTCCTCAGAGCGGGGTTCTCATCTTTGGG
AAGCAAGGCTCAGAGAAAACAATGTGGACATTGAAAAGGTCATGATTACAGACGAAGAGGAAATCA
GGACAACCAATCCCGTGGCTACGGAGCAGTATGGTTCTGTATCTACCAACCTCCAGAGAGGCAACCTA
GCAGACCAAGACTACACAAAACTGCTAGGCAAGCAGCTACCGCAGATGTCAACACACAAGGCGTTC
TTCCAGGCATGGTCTGGCAGGACAGAGATGTGTACCTTCCAGGGGCCATCTGGGCAAAGATTCCACAC
ACGGACGGACATTTTACCCCTCTCCCTCATGGGTGGATTCCGACTTAAACACCCTCTCCCCAGATT
CTCATCAAGAACACCCCGGTACCTGCGAATCCTTCGACCACCTTCAGTGCGGCAAAGTTTGCTTCTTC
ATCACACAGTACTCCACGGGACAGGTCAGCGTGGAGATCGAGTGGGAGCTGCAGAAGGAAAACAGCA
AACGCTGGAATCCCGAAATTCAGTACACTTCCAACATAACAAGTCTATTAATGTGGACTTTACTGTG
GACACTAATGGCGTGTATTTCAGAGCCTCGCCCCATTGGCACCAGATACCTGACTCGTAATCTGTAA
```

Payloads and promoters used in the study

For all subsequent experiments, the *CMV* promoter was replaced with a promoter known to be more robust in adult neurons. Cre recombinase and the GCaMP6f calcium sensor were driven by the human *Synapsin-1* (*hSyn1*) promoter; all of the fluorophores were driven by the *CAG* promoter; and the color-flipping construct was driven by the *EF1 α* promoter.

Virus production for the quantification of retrograde efficiency

hSyn-Cre payload was packaged using AAV1, AAV2, AAV5, AAV8, AAV9, DJ and AAV2-retro capsids at the Janelia Viral Shared Resource. All seven virus preparations were processed in parallel, and were titer matched before *in vivo* injections. All lots were diluted to the lowest measured titer (1.3E12 GC/ml), and each virus was injected into the right pontine nucleus of three adult *Rosa26-Lox-STOP-Lox-H2B-EGFP* mice (He et al., 2012).

Histology

Animals were sacrificed two to three weeks following virus injections, at which point the brains were harvested and the right hemisphere was sagittally sectioned at a thickness of 50 μ m. In the triple labeling experiment in Figure 1B and Movie S1, the fluorophores were antibody-amplified; otherwise, unstained sections were used. The sections were mounted in VECTASHIELD Antifade Mounting Medium containing DAPI (Vector Laboratories), and imaged using a P-E Panoramic slide scanner (3D Histech) using a 20x objective and FITC and DAPI filters.

When signal amplification was performed, the following antibody combinations were used: chicken anti-GFP (Rockland Immunochemicals) + goat anti-chicken IgY (H+L) Secondary Antibody Alexa Fluor® 488 (Invitrogen A11039); rabbit anti-RFP (Rockland Immunochemicals) + goat anti-rabbit IgG (H+L) Superclonal™ Secondary Antibody, Alexa Fluor® 555 (Invitrogen); mouse anti-FLAG (Rockland Immunochemicals) + goat anti-mouse IgG (H+L) Secondary Antibody, Alexa Fluor® 647 (Invitrogen). The sections were counterstained with Neurotrace (Invitrogen) and mounted in Aqua/Poly-Mount (Polysciences) before imaging.

Retrograde transport quantification

To quantify retrograde transport, the extent of corticopontine labeling was assessed in sagittal sections lateral to the injection tract (~1 mm lateral wrt midline) taken from *Rosa26-Lox-STOP-Lox-H2B-EGFP* animals injected in the basal pons with various AAV serotypes carrying Cre recombinase transgene. Images obtained with the Panoramic slide scanner were stitched together and then analyzed using custom software written in Matlab (Mathworks) to detect the GFP labeled nuclei across the cortex.

For each chosen sagittal section, a region of interest (ROI) was manually drawn around the cortex to isolate the area in the image for automated cell counting. To enhance the detection of nuclei, the image was then convolved with a “Mexican Hat” kernel comprising the difference of two Gaussians (26.00 μm variance and 3.25 μm variance). Image noise was reduced using a median filter, and basic peak detection was then performed. Linear density was computed as the number of labeled nuclei per mm of the total length of a line drawn manually to trace the outline of cortical layer V.

Quantification of local infection efficiency at the injection site

For rAAV2, rAAV9 and rAAV2-retro, additional analysis of infection efficiency at the injection site was performed. A single sagittal section spanning the middle of the injection site—as judged by the presence of extensive labeling along the injection tract—was chosen for each of the injected brains. The green channel was convolved with the “Mexican Hat” kernel (see above), and peaks were then detected as local maxima on these threshold images using custom functions written in Matlab. An ROI was drawn over the midbrain area containing the basal pontine nuclei but excluding the injection tract, and the total number of labeled nuclei within the ROI was tabulated.

Analysis of the generality of retrograde transport

Rosa26-Lox-STOP-Lox-H2B-EGFP mice were injected with 25 nl of rAAV2-retro *hSyn1-Cre* (1.3E12 GC/ml) in the dorsal striatum. Three weeks after injection, coronally-sectioned brains were imaged using a Panoramic Scanner to visualize DAPI stained nuclei and green fluorescence from H2B-GFP expressing nuclei. The green channel was similarly used for the detection of labeled nuclei (see above). The blue channel of each section was aligned to the Nissl images from the Allen Brain Institute’s standardized mouse brain atlas using custom analysis routines written with the help of the Matlab Image Processing Toolbox. The annotated regions from the ABI’s mouse brain atlas were then used to assign detected neurons in aligned sections to specific brain regions (Kuan et al., 2015).

We note that finite precision of the reference atlas together with anatomical variability of individual brains limit the robustness of this semi-automated process to prominent afferent inputs.

Heparin binding assay

The heparin affinity of rAAV2-retro and wild-type AAV2 were analyzed as previously described (Jang et al., 2011). Briefly, approximately 10^{11} purified genomic particles were loaded onto a 1 ml HiTrap heparin column (GE Healthcare Sciences, Piscataway, NJ) previously equilibrated with 150 mM NaCl and 50 mM Tris at pH 7.5. Elution was then performed by increasing the concentration of NaCl in steps of 50 mM up to a final concentration of 950 mM, followed by a wash with 1M NaCl. A small fraction of each elution was used to infect HEK293T cells, and the percentage of GFP positive cells was quantified 48 hours post-infection using a Guava EasyCyte 6HT flow cytometer (EMD/Millipore).

Imaging of neuronal population activity *in vivo* following retrograde delivery of GCaMP6f

Seven adult mice were anesthetized with isoflurane (2%) and placed in a stereotactic frame (Kopf Instruments; Tujunga, CA) on a 37°C heating pad. The scalp and periosteum over the skull were removed, a layer of UV-curing OptiBond adhesive (Kerr; Orange, CA) was applied, and a custom-made headpost (Osborne and Dudman, 2014) was affixed with dental cement. rAAV2-retro carrying a *hSyn1-GCaMP6f* (1.0×10^{13} GC/ml) payload was injected into the basal pontine nuclei (BPN) (3.9 mm posterior and 0.4 mm lateral to Bregma, depths 5.8, 5.6 and 5.4 mm, 100 nl at each depth) using a Nanoliter 2010 injector (World Precision Instruments). A cranial window (one 170 μm -thick pane of laser-cut glass, 2 mm diameter) was placed over the primary motor cortex (centered on 0.7 mm anterior and 1.6 mm lateral to Bregma).

Following surgery, injections of ketoprofen (5 mg/kg) and buprenorphine (0.1 mg/kg; Henry Schein Animal Health; Melville, NY) were administered subcutaneously. Mice were allowed to recover for one-week following surgery and then were imaged briefly under a 2-photon microscope to assess virus expression. All animals had visually identified GCaMP6f expressing cells in layer V of M1 one-week post injection. Then the animals were habituated to head fixation in a custom-built apparatus and trained to retrieve a food pellet as previously described (Guo et al., 2015).

GCaMP6f was excited at 920 nm (typically 20–40 mW at the back aperture) with a Ti:Sapphire laser (Chameleon, Coherent) and imaged through a Nikon 16x, 0.8-N.A. objective. Emission light passed

through a 565 nm DCXR dichroic filter (Chroma Technology) and an ET525/70 nm m-2p filter (Chroma Technology) and was detected by a GaAsP photomultiplier tube (10770PB-40, Hamamatsu). Images (512 × 512 pixels) were acquired at ~30 Hz with resonating scanners using ScanImage software.

CRISPR/Cas9 genome editing

The *CMV* promoter in pAAV-*CMV*-SaCas9-empty (Slaymaker et al., 2016) was replaced with *hSyn1* to generate pAAV-*hSyn1*-SaCas9-empty. Oligonucleotides encoding sgRNA protospacer sequences were custom ordered, phosphorylated, hybridized and ligated into the *BsaI* restriction sites of pAAV-*hSyn1*-SaCas9-empty to generate pAAV-*hSyn1*-SaCas9-tdTomato-1 to -10. Oligonucleotide sequences used were:

tdTomato sgRNA 1 Fwd

CACCGCAAGGGCGAGGAGGTCATCA

tdTomato sgRNA 1 Rev

AAACTGATGACCTCCTCGCCCTTGC

tdTomato sgRNA 2 Fwd

CACCGTGGAGGGCTCCATGAACGGCC

tdTomato sgRNA 2 Rev

AAACGGCCGTTTCATGGAGCCCTCCAC

tdTomato sgRNA 3 Fwd

CACCGAGGACGGCGGCCACTACCTGG

tdTomato sgRNA 3 Rev

AAACCCAGGTAGTGGCCGCCGTCCTC

tdTomato sgRNA 4 Fwd

CACCGACAACAACATGGCCGTCATCA

tdTomato sgRNA 4 Rev

AAACTGATGACGGCCATGTTGTTGTC

tdTomato sgRNA 5 Fwd

CACCGAAGGACGGCGGCCACTACCTGG

tdTomato sgRNA 5 Rev

AAACCCAGGTAGTGGCCGCCGTCCTTC

tdTomato sgRNA 6 Fwd

CACCGACAACAACATGGCCGTCATCA

tdTomato sgRNA 6 Rev

AAACTGATGACGGCCATGTTGTTGTC

tdTomato sgRNA 7 Fwd

CACCGGTCACCTTCAGCTTGGCGGT

tdTomato sgRNA 7 Rev

AAACACCGCCAAGCTGAAGGTGACC

tdTomato sgRNA 8 Fwd

CACCGCCGTACATGAACTGGGGGGA

tdTomato sgRNA 8 Rev

AAACTCCCCCAGTTCATGTACGG

tdTomato sgRNA 9 Fwd

CACCGTCTTGTAATCGGGGATGTCGG

tdTomato sgRNA 9 Rev

AAACCCGACATCCCCGATTACAAGAC

tdTomato sgRNA 10 Fwd

CACCGCCGTCCTGCAGGGAGGAGTC

tdTomato sgRNA 10 Rev

AAACGACTCCTCCCTGCAGGACGGC

The ability of each oligo to direct genome editing was first evaluated *in vitro*. Neuro2A cells were transfected with 800 ng of pAAV-*hSyn1*-SaCas9-tdTomato-1 to -10, 100 ng of pAAV-FLEX-CAG-tdTomato and 100 ng of pAAV-CAG-EGFP using polyethylenimine. At 72 hrs after transfection, cells were harvested and ~70,000 EGFP positive Neuro2A cells were isolated by fluorescence activated cell sorting (FACS) using a BD Influx Sorter (BD Biosciences). Genomic DNA was then extracted, and the frequency of tdTomato gene modification was evaluated by the Surveyor nuclease assay (Integrated DNA Technologies) as previously described (Cong et al., 2013). sgRNA 7—one of two that appeared to direct

two cleavage events within the tdTomato sequence—was packaged into AAV2-retro and used for *in vivo* genome editing.

~100 nl of rAAV2-retro-*hSyn1*-SaCas9-anti-tdTomato (5.0 E13 GC/ml) or rAAV2-retro-*hSyn1*-SaCas9-empty was then injected into the BPN of *Rbp4_KL100* Cre × tdTomato mice as described above. Six weeks after injections, brains were harvested and 40 μm-thick coronal sections were cut and stained against the HA-tagged Cas9 (anti-HA antibody C29F4 from Cell Signaling, diluted 1:1600; secondary antibody: donkey anti-mouse Alexa Fluor 488, from Jackson ImmunoResearch, diluted 1:250) and against the NeuN neuronal marker (anti-NeuN antibody A60 from Millipore, diluted 1:250; secondary antibody: donkey anti-rabbit Alexa Fluor 647 A-31573, from ThermoFisher, diluted 1:500). Following antibody staining, the sections were mounted onto slides with VECTASHIELD Antifade Mounting Medium containing DAPI (Vector Laboratories) and visualized using a Zeiss Axio Observer A1 inverted microscope (Zeiss). Quantification of immunostaining was performed using ImageJ analysis software (NIH).

REFERENCES

- Cong, L., Ran, F.A., Cox, D., Lin, S., Barretto, R., Habib, N., Hsu, P.D., Wu, X., Jiang, W., and Marraffini, L.A. (2013). Multiplex genome engineering using CRISPR/Cas systems. *Science* 339, 819-823.
- He, M., Liu, Y., Wang, X., Zhang, M.Q., Hannon, G.J., and Huang, Z.J. (2012). Cell-type-based analysis of microRNA profiles in the mouse brain. *Neuron* 73, 35-48.
- Jang, J.-H., Koerber, J.T., Kim, J.-S., Asuri, P., Vazin, T., Bartel, M., Keung, A., Kwon, I., Park, K.I., and Schaffer, D.V. (2011). An evolved adeno-associated viral variant enhances gene delivery and gene targeting in neural stem cells. *Molecular Therapy* 19, 667-675.
- Koerber, J.T., Jang, J.-H., and Schaffer, D.V. (2008). DNA shuffling of adeno-associated virus yields functionally diverse viral progeny. *Molecular Therapy* 16, 1703-1709.
- Koerber, J.T., Klimczak, R., Jang, J.-H., Dalkara, D., Flannery, J.G., and Schaffer, D.V. (2009). Molecular evolution of adeno-associated virus for enhanced glial gene delivery. *Molecular Therapy* 17, 2088-2095.
- Kuan, L., Li, Y., Lau, C., Feng, D., Bernard, A., Sunkin, S.M., Zeng, H., Dang, C., Hawrylycz, M., and Ng, L. (2015). Neuroinformatics of the allen mouse brain connectivity atlas. *Methods* 73, 4-17.
- Maheshri, N., Koerber, J.T., Kaspar, B.K., and Schaffer, D.V. (2006). Directed evolution of adeno-associated virus yields enhanced gene delivery vectors. *Nature biotechnology* 24, 198-204.
- Müller, O.J., Kaul, F., Weitzman, M.D., Pasqualini, R., Arap, W., Kleinschmidt, J.A., and Trepel, M. (2003). Random peptide libraries displayed on adeno-associated virus to select for targeted gene therapy vectors. *Nature biotechnology* 21, 1040-1046.
- Slaymaker, I.M., Gao, L., Zetsche, B., Scott, D.A., Yan, W.X., and Zhang, F. (2016). Rationally engineered Cas9 nucleases with improved specificity. *Science* 351, 84-88.